WL-TR-94-3156

Analysis and Characterization of Measured Aerodynamic Loadings on a Tactical Missile

Mark S. Ewing
Department of Aerospace Engineering
and
Farshid Haste
Department of Mechanical Engineering
University of Kansas
Lawrence KS

March 1995

Final Report for Period April 1994 - November 1994

Approved for public release; distribution unlimited.

19950519 003

Flight Dynamics Directorate
Wright Laboratory
Air Force Materiel Command
Wright-Patterson Air Force Base, Ohio 45433-7542

NOTICE

When Government drawings, specification, or other data are used for any purpose other than in connection with a definitely Government-related procurement, the United States Government incurs no responsibility or any obligation whatsoever. The fact that the Government may have formulate or in any way supplied the said drawings, specification, or other data, is not to be regarded by implication, or otherwise in any manner construed, as licensing the holder, or any other person or corporation, or as conveying any rights or permission to manufacture, use, or sell any patented invention that may in any way be related thereto.

This report is releasable to the National Technical Information Service (NTIS). At NTIS, it will be available to the general public, including foreign nations.

This technical report has been reviewed and is approved for publication.

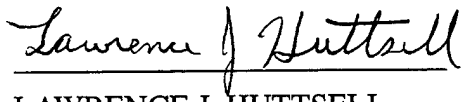

LAWRENCE J. HUTTSELL
Aerospace Engineer
Aeroelasticity Section
Structural Dynamics Branch

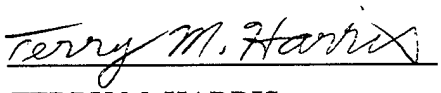

TERRY M. HARRIS
Technical Manager
Aeroelasticity Section
Structural Dynamics Branch

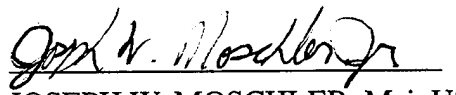

JOSEPH W. MOSCHLER, Maj, USAF
Chief, Structural Dynamics Branch
Structures Division

If your address has changed, if you wish to be removed from our mailing list, or if the addressee is no longer employed by your organization, please notify, WL/FIBGE, Bldg 45, 2130 Eighth St Ste 1, WPAFB OH 45433-7542 to help us maintain a current mailing list.

Copies of this report should not be returned unless return is required by security consideration, contractual obligations, or notice on a specific document.

REPORT DOCUMENTATION PAGE

Form Approved
OMB No. 0704-0188

1. AGENCY USE ONLY (Leave blank)	2. REPORT DATE	3. REPORT TYPE AND DATES COVERED
	March 1995	Final Report April 1994 - November 1994

4. TITLE AND SUBTITLE
Analysis and Characterization of Measured Aerodynamic Loading on a Tactical Missile

5. FUNDING NUMBERS
PE: 2401
TA: LE
WU: 00

6. AUTHOR(S)
Mark S. Ewing and Farste Haste

7. PERFORMING ORGANIZATION NAME(S) AND ADDRESS(ES)
University of Kansas
Lawrence KS

8. PERFORMING ORGANIZATION REPORT NUMBER

9. SPONSORING / MONITORING AGENCY NAME(S) AND ADDRESS(ES)
Flight Dynamics Directorate
Wright Laboratory
Air Force Materiel Command
Wright Patterson AFB OH 45433-7542

10. SPONSORING / MONITORING AGENCY REPORT NUMBER
WL-TR-94-3156

11. SUPPLEMENTARY NOTES

12a. DISTRIBUTION / AVAILABILITY STATEMENT
Approved for public release; distribution unlimited

12b. DISTRIBUTION CODE

13. ABSTRACT *(Maximum 200 words)*

A tactical missile instrumented with pressure and acceleration sensors was flown on a fighter aircraft to help characterize the "in carriage" flight environment. The pressure data have been analyzed with various techniques to determine if a simple, yet appropriate, model can be used to model forces applied to a structural finite element model. Analysis has revealed a nearly uniform "convection" of narrow-band random forces along the missile, indicating a highly coherent aerodynamic structure. The circumferential distribution of the standard deviation of measured pressures which tend to "swirl" along the missile seem to indicate the existence of shed vortex-related "swirl" of the aerodynamic excitation.

14. SUBJECT TERMS
unsteady aerodynamics, pressure data, experimental, dynamic loads, missile

15. NUMBER OF PAGES
51

16. PRICE CODE

17. SECURITY CLASSIFICATION OF REPORT	18. SECURITY CLASSIFICATION OF THIS PAGE	19. SECURITY CLASSIFICATION OF ABSTRACT	20. LIMITATION OF ABSTRACT
UNCLASSIFIED	UNCLASSIFIED	UNCLASSIFIED	UNCLASSIFIED

TABLE OF CONTENTS

LIST OF FIGURES

1.0 INTRODUCTION

The Advanced Medium-Range Air-to-Air Missile (AMRAAM), shown in Figure 1, often encounters a severe aerodynamic environment during external carriage on fighter aircraft. This environment is especially harsh for missiles located close to an engine inlet during a high angle of attack maneuver which involves a throttle chop. In such a case, inlet corner vortices are known to "spill" out of the inlet (forming a "horseshoe" vortex). The vortex map at the plane of the engine inlet is depicted in Figure 2. Concern over the ability to predict missile response in such conditions has spawned research on the prediction of the associated aerodynamics. Companion research efforts include the development of instrumented missiles to measure in-flight pressures [1] and efforts to determine the response of tactical missiles [2].

In the late 1980s, an AMRAAM was modified to serve as a digital measurement vehicle (DMV) by personnel from the Structural Dynamics Branch, Structures Division of Wright Laboratory's Flight Dynamics Directorate (WL/FIBG at that time). Mr. Richard "Dick" Talmadge was the program manager. The DMV was fitted with accelerometers and pressure transducers, then flown in a number of flight tests to determine if the digital technology and a newly developed miniature tape recorder could be shown to be preferable to the analog system flown earlier.

The pressure transducers were located at the stations and locations indicated in Figure 3. The intent was to provide pressure measurements at three nearly equally spaced positions around the missile at the five selected longitudinal stations. However, the location of structures within the missile limited the available locations. The pressure transducers used were flush-mounted "Kulites."

After the flight tests were flown, an analytical effort was begun to determine if the aerodynamic environment could be characterized to the extent that structural responses could be predicted from the measured pressure excitations [2]. The basis for measuring success was a direct comparison with the measured accelerations. Unfortunately, the level of success was not as expected, prompting the effort reported here. The major problem with the earlier study was that no clear physical model of the aerodynamics was available, and a somewhat "brute force" method of applying loads was attempted. Another problem was that there was some uncertainty in the modelling of the elasticity of the connections between the missile and the launcher in the earlier study. An on-going analysis takes into account the improved aerodynamic load modelling reported here as well as more realistic modelling of the missile support conditions.

2.0 RECORDED DATA

The DMV was flown for a number of flights on the F-15 LAU-106 ejector launcher mounted at (forward fuselage) station number 7. The PCM data from the DMV tape recorder were digitized and calibrated by Mr. Dansen Brown of the Data Analysis Group. Under the sponsorship of Major Kevin Dougherty of the AMRAAM program office (ASC/YAJ, Eglin AFB) two sets of data were

made available to the authors. The flight condition selected for analysis is from flight I-1157-88, flown on 10 December 1990, at Eglin AFB, Florida.

Flight point 7 was a "wind-up turn" with a throttle chop, beginning at flight time 20:31:55.00. The conditions were:

Mach number	0.89
altitude	20.1 K feet
dynamic pressure	537.0
angle of attack	8.6 degrees

The pressure-time histories for flight point 7 are given in Appendix A. Auto-power spectral densities are given in Appendix B.

3.0 ANALYSIS

3.1 Analysis Using Amplitude Statistics of the Excitation

A very simplistic way to look at the recorded data is to simply calculate statistical measures of the excitation across the missile. Without knowing the nature of the pressure field *a priori*, it may be true that the number of pressure transducers required to characterize the pressure field well enough for structural analysis is much larger than available on the DMV. Without a comparative measurement density study, however, there is no way to know. In this study, the approach is taken that one plausible way to characterize the excitation is to fit polynomial curves through measurement levels around the missile and along the missile in order to see if any identifiable patterns emerge. Further, rather than fitting curves through pressures at instants in time (a most exhaustive pursuit), the curves were fit through the means and standard deviations of the excitation pressures. The idea is that flow "structures" in the excitation would emerge from these measures if they were strong aerodynamic structures. It was expected at the outset that regions on the missile experiencing large standard deviations of excitation would be "bathed" by inlet vortices, while relatively quiet regions were not. The presence of such "excitation segregation," then would indicate a steady vortex, such as the "horseshoe" vortex known to often spill out of a rectangular engine inlet.

Two types of means and standard deviations have been computed. First, using an ensemble of 40,000 pressure measurements, 40 time slices of 1000 records were used to compute the standard deviations and means at each of the measurement locations. A set of 5th degree polynomial curves were then fit through the 3 computed values at each missile station. This results in a set of 5 curvefits each for standard deviation and mean depicting the distribution of pressure around the missile at a given missile station. These distributions are shown as carpet plots in Figures 4 and 8. Note that the distribution of standard deviation seems to have more structure and much higher magnitude than the mean. The distribution of standard deviation and mean around the missile for the 40th time slice is given in Figures 5 and 9 in both linear and polar form. From these plots, it was hoped that an identifiable "swirl" would be apparent, for instance a clear direction of rotation

which is proportional to the distance along the missile. However, this is difficult to substantiate at this time. On the other hand, it is noted that the magnitude of the standard deviation at stations 32 and 66 are nearly twice that at 16 and 90, and a clockwise flow (looking aft) may be indicated.

The second type of computations were the calculation of *running* standard deviation and mean. For instance, the 17th set of curvefits represented the standard deviation and mean of the first 17,000 measurements (17 time slices *times* 1000 measurements per time slice). Carpet plots are given in Figures 6 and 10. Figures 7 and 11 give the distribution of standard deviation and mean for the whole ensemble of data.

3.2 Analysis Using Phase Relationships of the Excitation

The knowledge that the AMRAAM often experiences severe "wash" from engine air "dumping" during a throttle chop suggests that significant aerodynamic disturbances are "convected" along the missile at a speed near the flight speed of the aircraft. Therefore, from the missile point of view, the narrow-band random excitation is very much temporally correlated. That is, a force or collection of forces arriving at a downstream point is just a time-delayed version of what an upstream point already experienced. If the excitation also swirls, as in a shed vortex, the convection can be along a helical rather than a lineal path. A straightforward way to identify a convected, or spatially correlated, excitation is to observe the temporal correlation function relating two pressures or the phase relationship in their cross power spectrum. The theory of this concept will now be presented based on the excellent text by Bendat and Pearsol [3].

When a single force moves at a constant velocity across the boundary of a structure, it will be recorded at discrete measurement locations with an arrival time varying in direct proportion to the distance between the points (and inversely proportional to the velocity). In other words there is a delay, with respect to an "upstream" recording location, in the arrival time for a "downstream"

$$\tau = d/c \tag{1}$$

recording location. The calculation of the temporal delay is very simply calculated as:
where d is the distance between a reference point "upstream" from a disturbance (force) moving toward a point of interest, and c is the velocity with which it moves.

The delay in arrival of an excitation at one point with respect to another results in a couple of interesting relationships. Consider first, the cross-correlation function between two functions, x(t) and y(t), defined by:

$$R_{xy}(\tau) = \lim_{T\to\infty} \frac{1}{T}\int_0^T x(t)y(t+\tau)dt \tag{2}$$

Here T is the time period over which the function is calculated. Now consider the cross-power

spectral densities of the two signals discussed above. The cross-power spectral density is:

$$S_{ij}(f) = \int_{-\infty}^{\infty} R_{ij}(\tau) e^{-i2\pi f\tau}\, d\tau \qquad (3)$$

Here f is the frequency. Finally, the phase angle in terms of a time delay is given by:

$$\theta = 2\pi f\tau \qquad (4)$$

To summarize, then, the correlation between two measurement locations subject to a force moving past them both can be described in terms of a *delay* in the time domain or a *phase change* in the frequency domain.

Figures 12-20 show the *phase* of the cross power spectral density of nine measurement pairs near the front of the DMV, namely:

sensor 2 and sensors 5, 6 and 7
sensor 5 and sensors 9, 10 and 11
sensor 2 and sensors 9, 10 and 11

Note the nearly linearly varying phase angle in the cross-power spectral density in the 200 to 500 Hz frequency range for most measurement pairs. This is exactly what is expected according to theory. Moreover, the "slope" of the phase change is generally in agreement with theory, that is, that the measurement locations furthest apart have the greatest rate of phase angle change (because the time delay is greater). The analysis of this data is on-going, with the hope that computational fluid dynamics (CFD) analysis will be able to shed light on the presence of vortex structures in the vicinity of the engine inlet.

4.0 CONCLUSION AND RECOMMENDATIONS

The presence of temporal correlation in the flow past a missile near an engine inlet consistent with swirling convection has been identified by analysis of measured pressures on a missile. The demonstration was based on both cross-power spectra phase shift analysis (for the convection) and on statistical analysis of curvefitted measurements (for the swirl).

Cooperative research with CFD analysts is clearly indicated if a better view of flow near an engine inlet is to be realized. Also, measurement programs with a more dense pressure transducer network may be necessary. Recent advances in the miniaturization of flight-quality measurement systems makes this entirely feasible.

5.0 REFERENCES

1. "AMRAAM Instrument Measurement Vehicle (IMV) Captive Flight Test Report", 32050-2963, February 1986 (CDRL A03S, Contract no. F08635-82-C-0001), Hughes Aircraft Company (Hughes Ref. No. E76091, MSG 51226).

2. "AMRAAM Model User's Guide," Deliverable 3 from GSA task, "Model Prediction of AMRAAM Vibration Levels," GSA Contract Report No. GS00K88AFD2587, GSA Task Order CCC571625, Dayton Operations of Atlantic Research Corporation, 4 June 1991.

3. Bendat, J. S. and Pearsol, A.G., Engineering Applications of Correlation and Spectral Analysis, John Wiley & Sons, 1980.

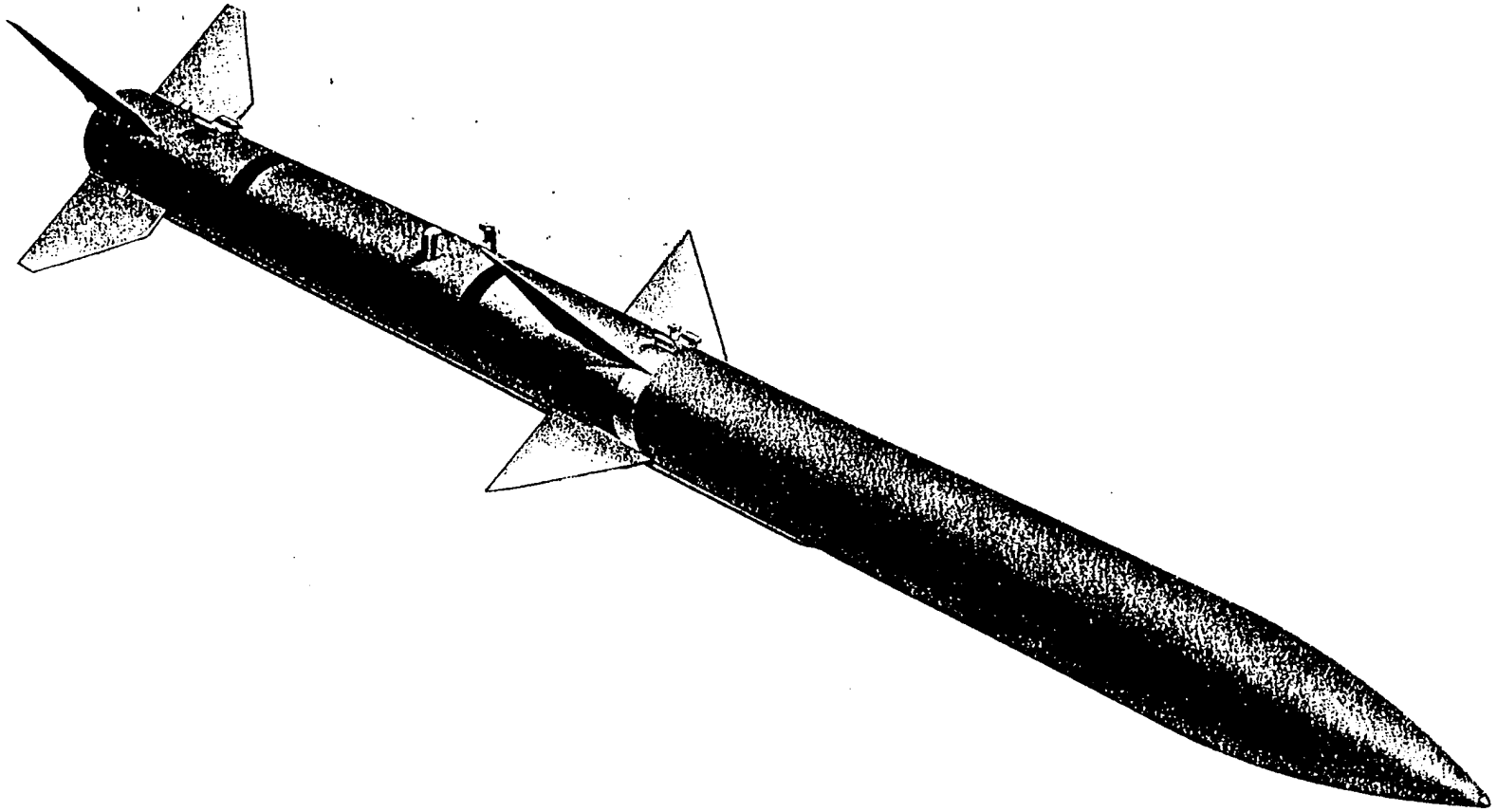

Figure 1. Perspective view of AMRAAM.

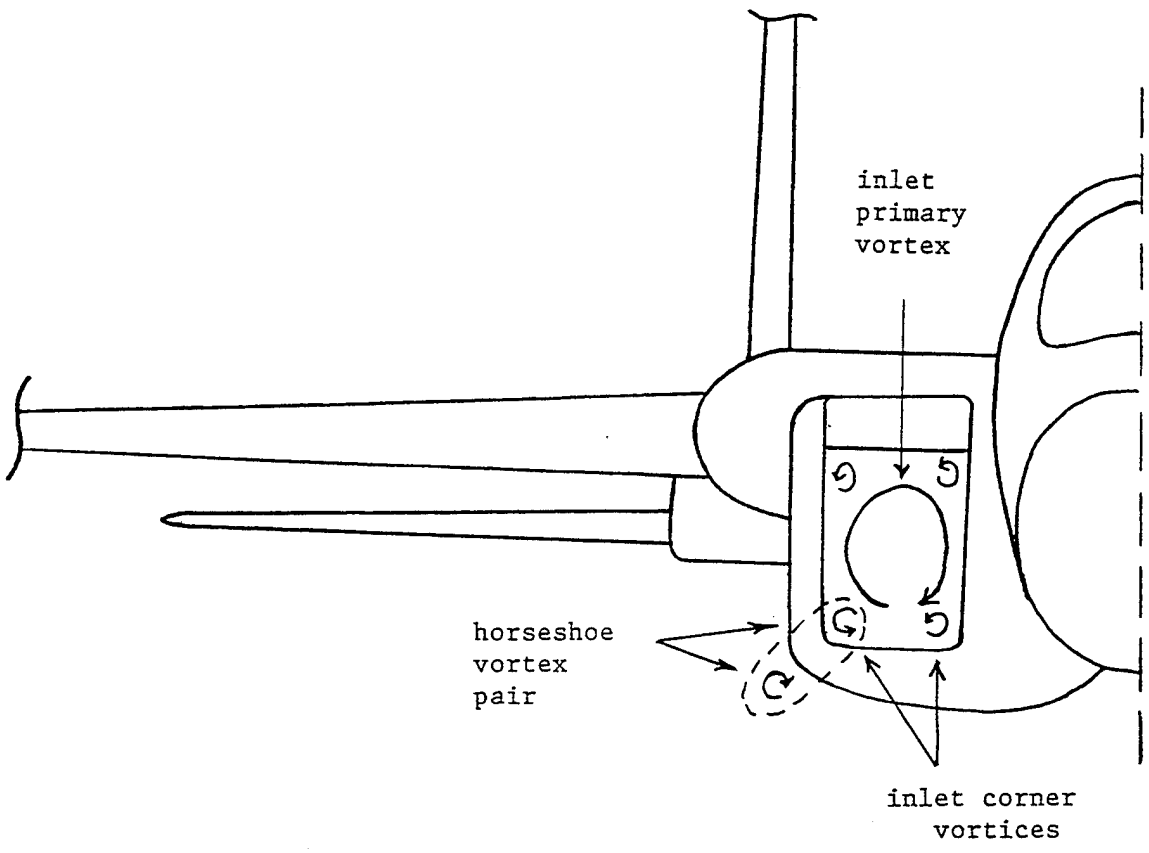

Figure 2. F-15 inlet vortices diagram.

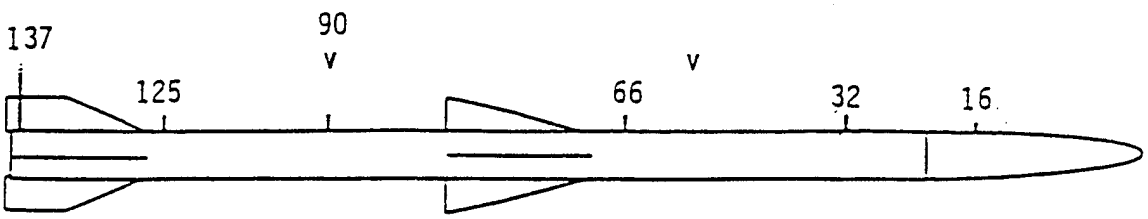

(a) Station Locations

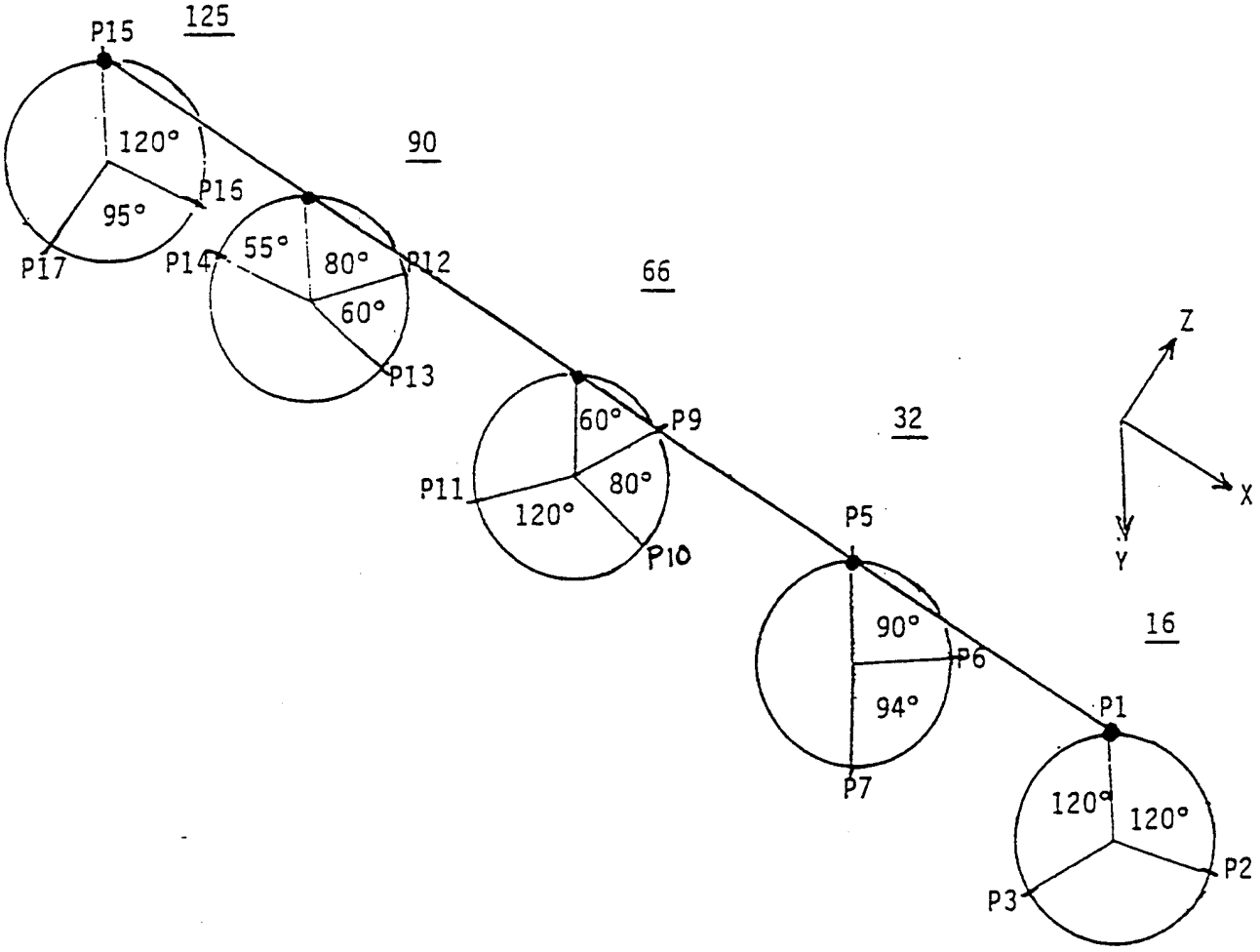

(b) Pressure Measurement Locations at Each Station

Figure 3. DMV pressure measurement locations.

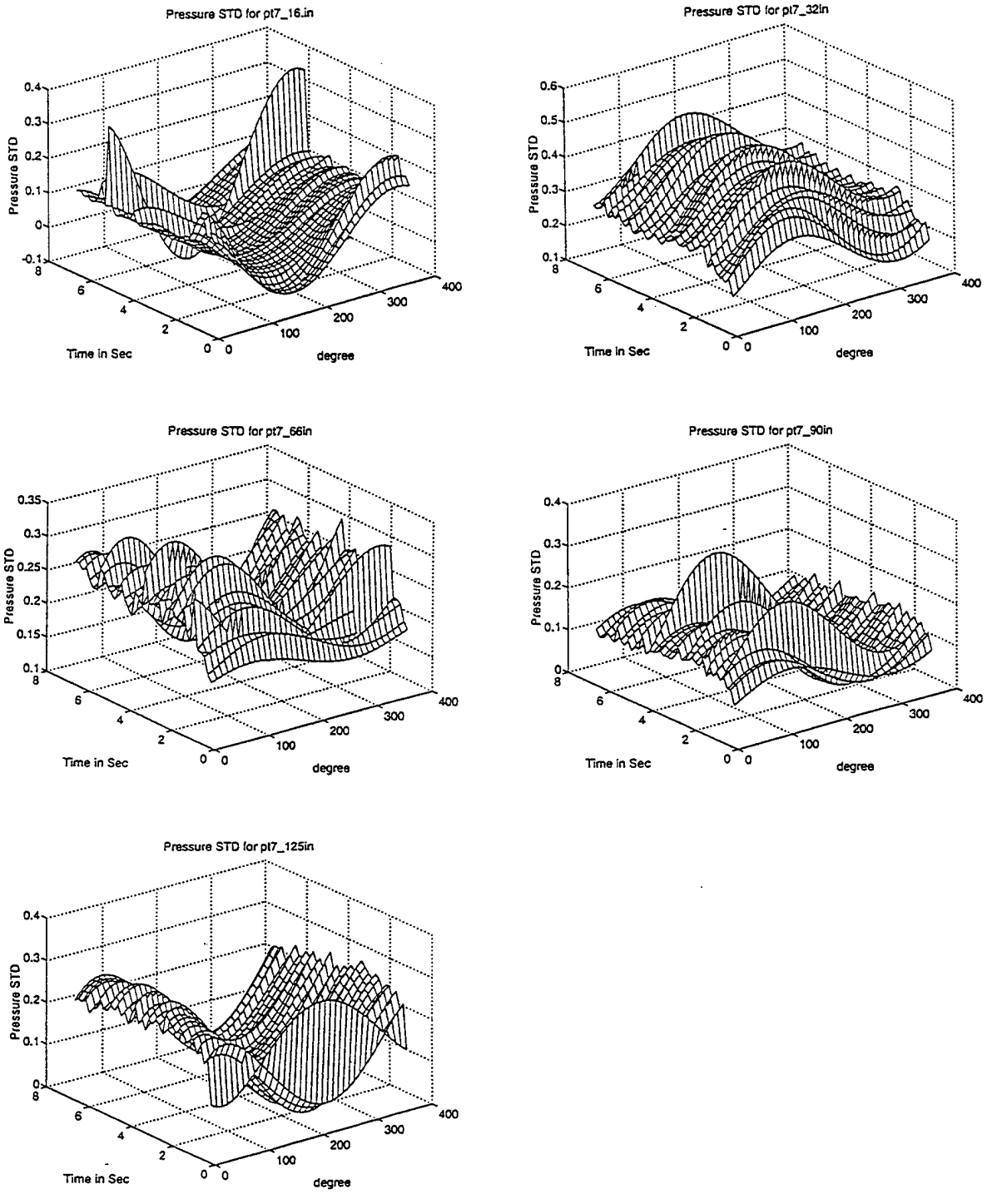

Figure 4. Curvefits (around the DMV) of pressure standard deviations of 40 successive 1000-sample time slices.

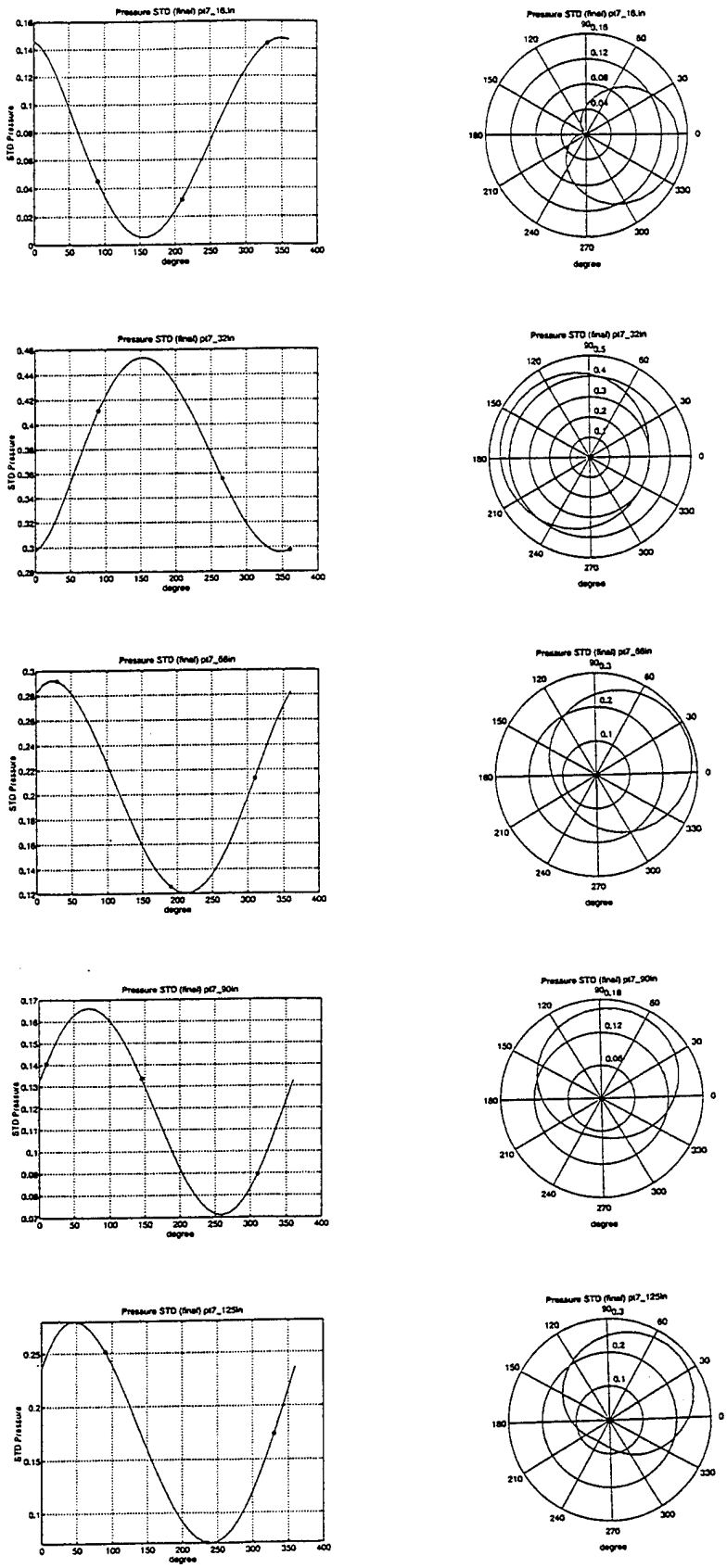

Figure 5. Curvefit of pressure standard deviation for the final 1000-sample time slice.

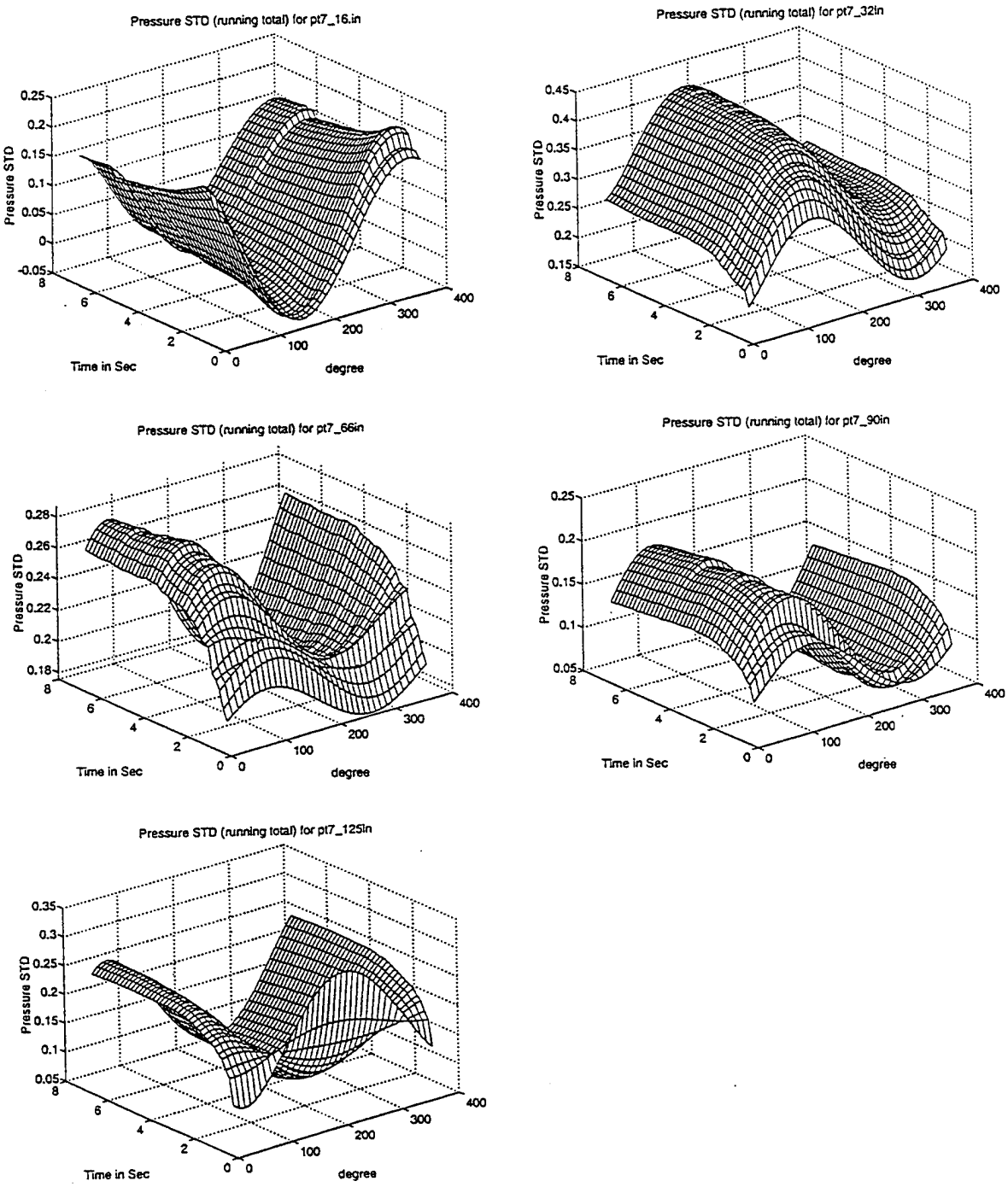

Figure 6. Curvefits of the evolving pressure standard deviation for 40,000 samples.

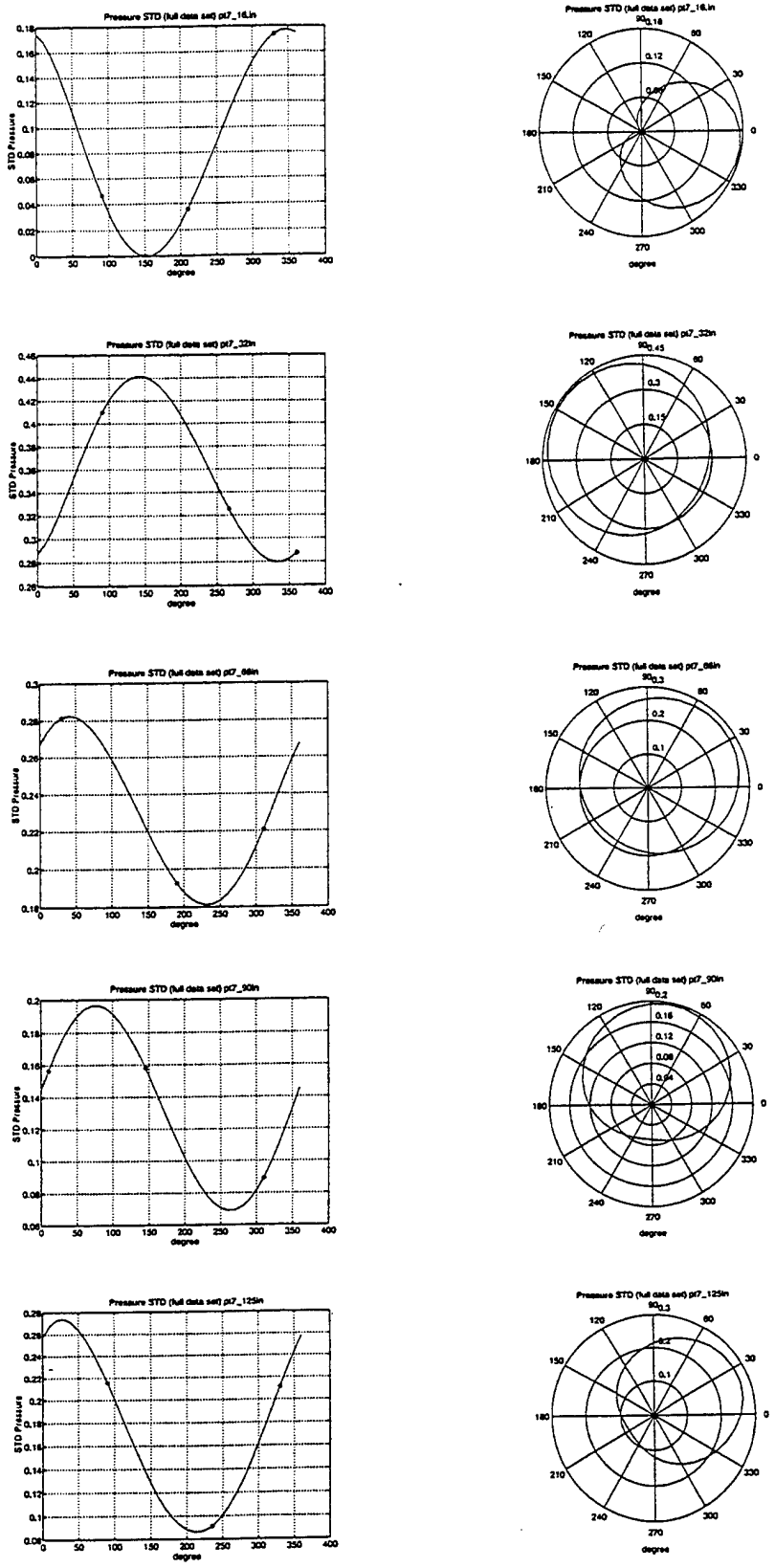

Figure 7. Curvefit of the pressure standard deviation for 40,000 samples.

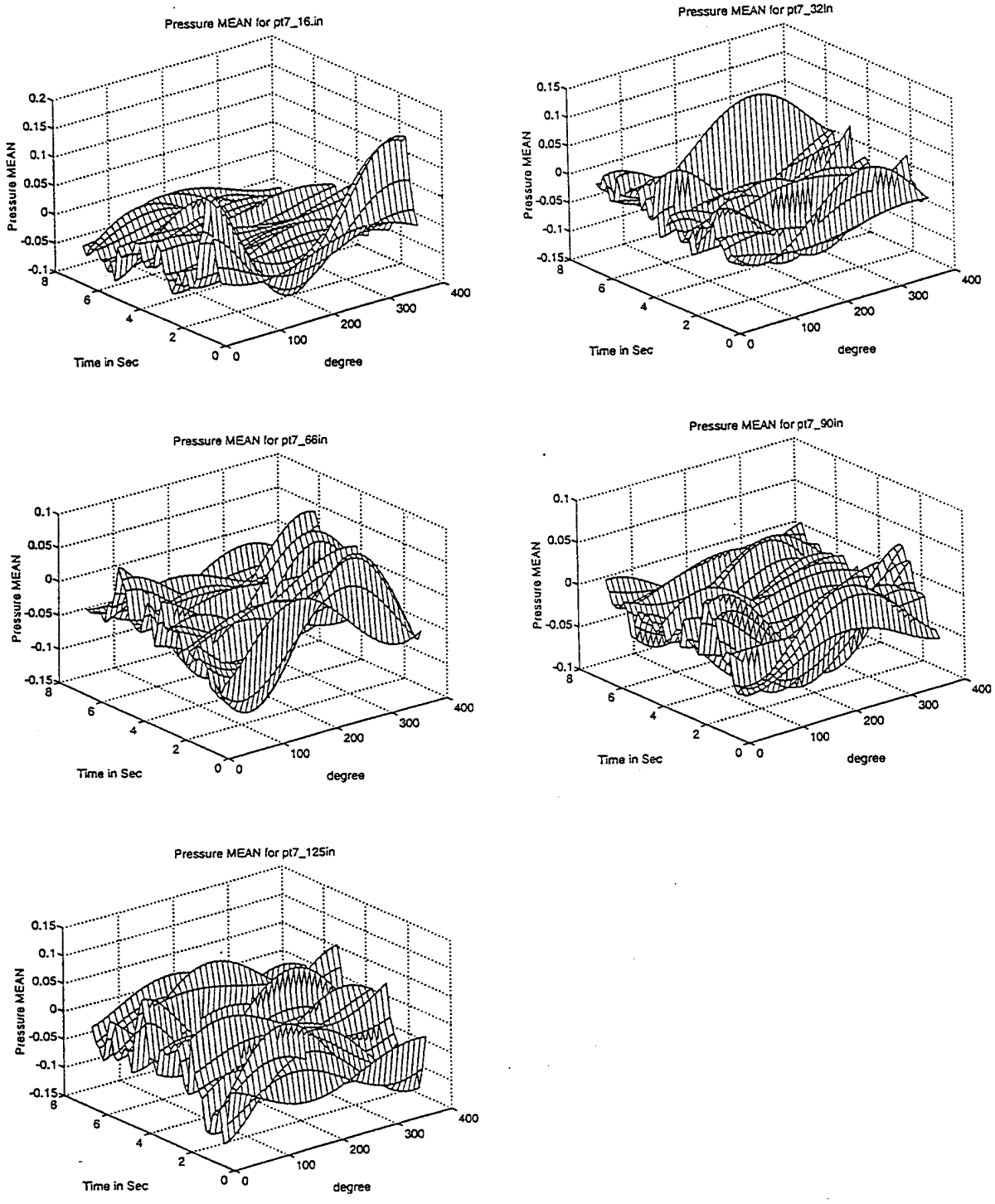

Figure 8. Curvefits of pressure mean for 40 successive 1000-sample time slices.

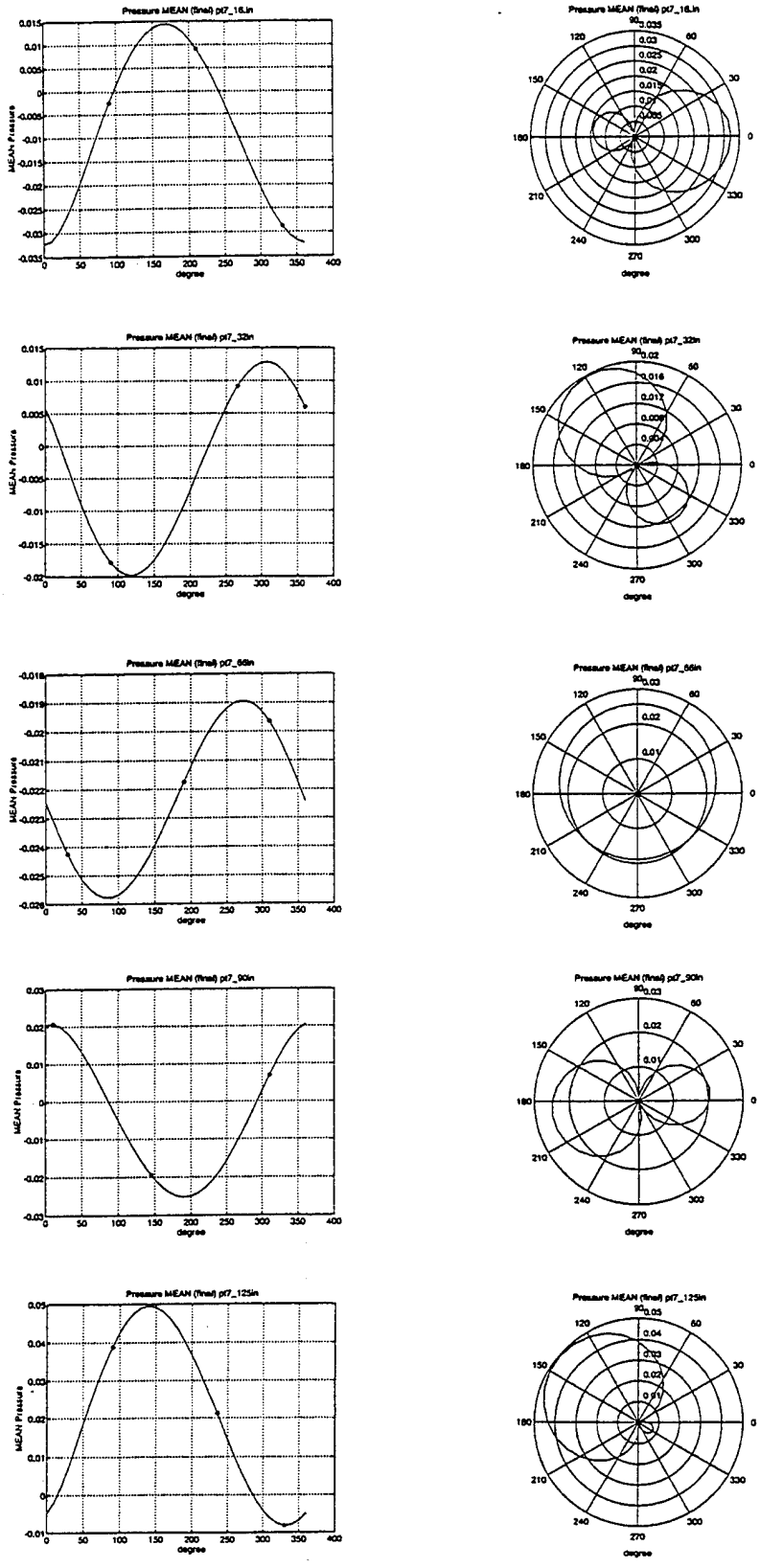

Figure 9. Curvefit of pressure mean for the final 1000-sample time slice.

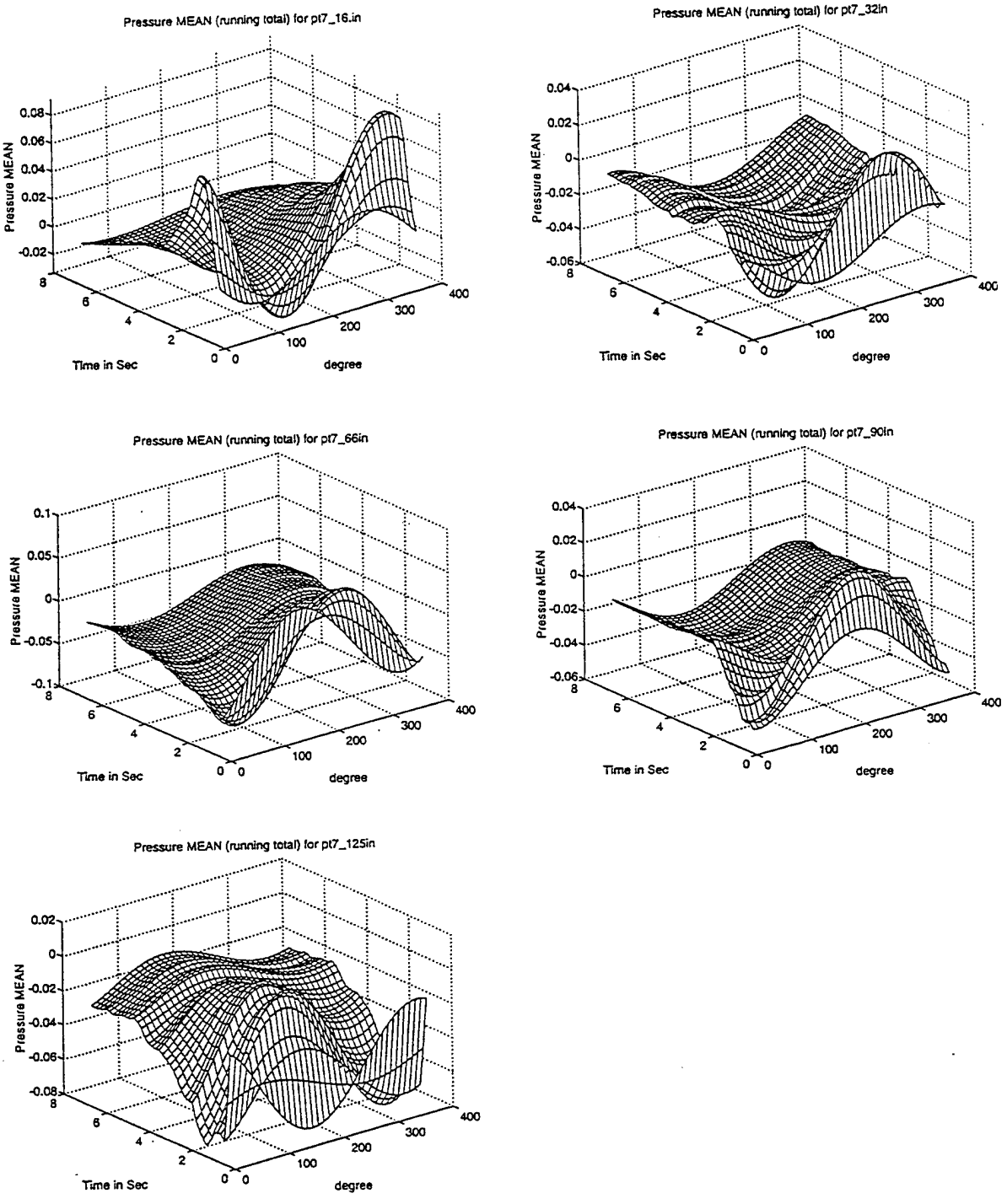

Figure 10. Curvefits of the evolving pressure mean for 40,000 samples.

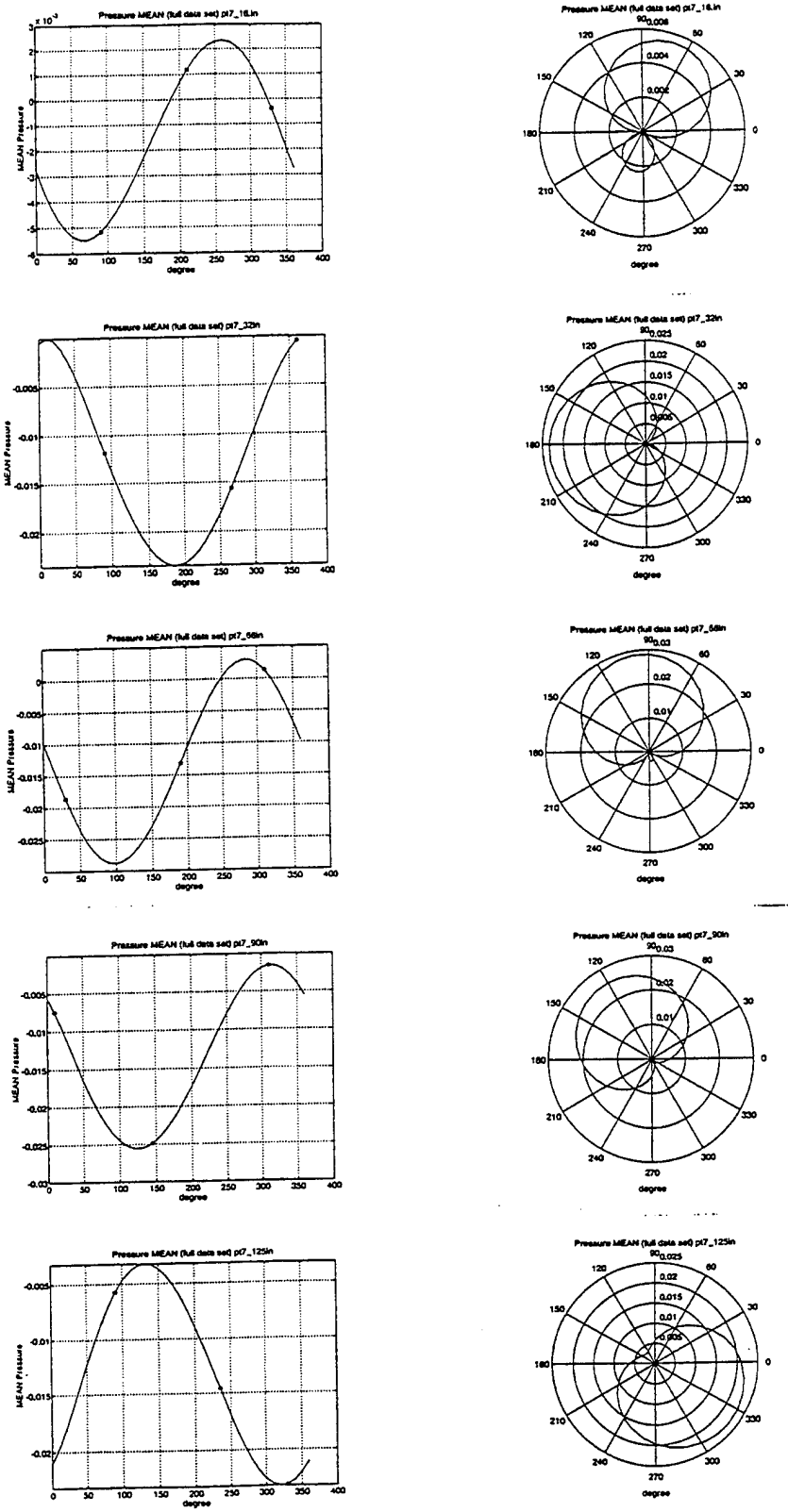

Figure 11. Curvefit of the pressure mean for 40,000 samples.

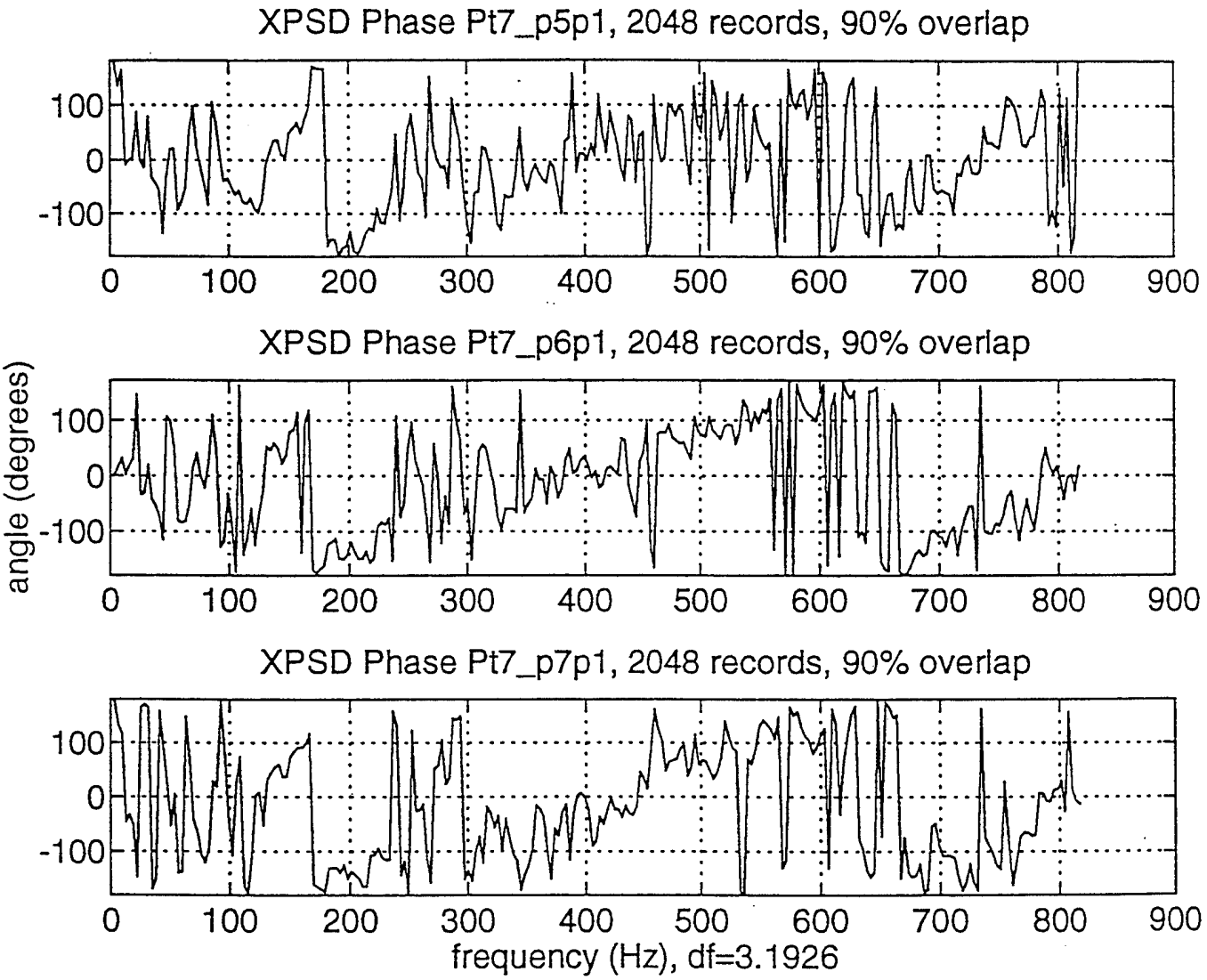

Figure 12. Phase of pressure cross-PSDs relating measurement points 5,6 & 7 to 1.

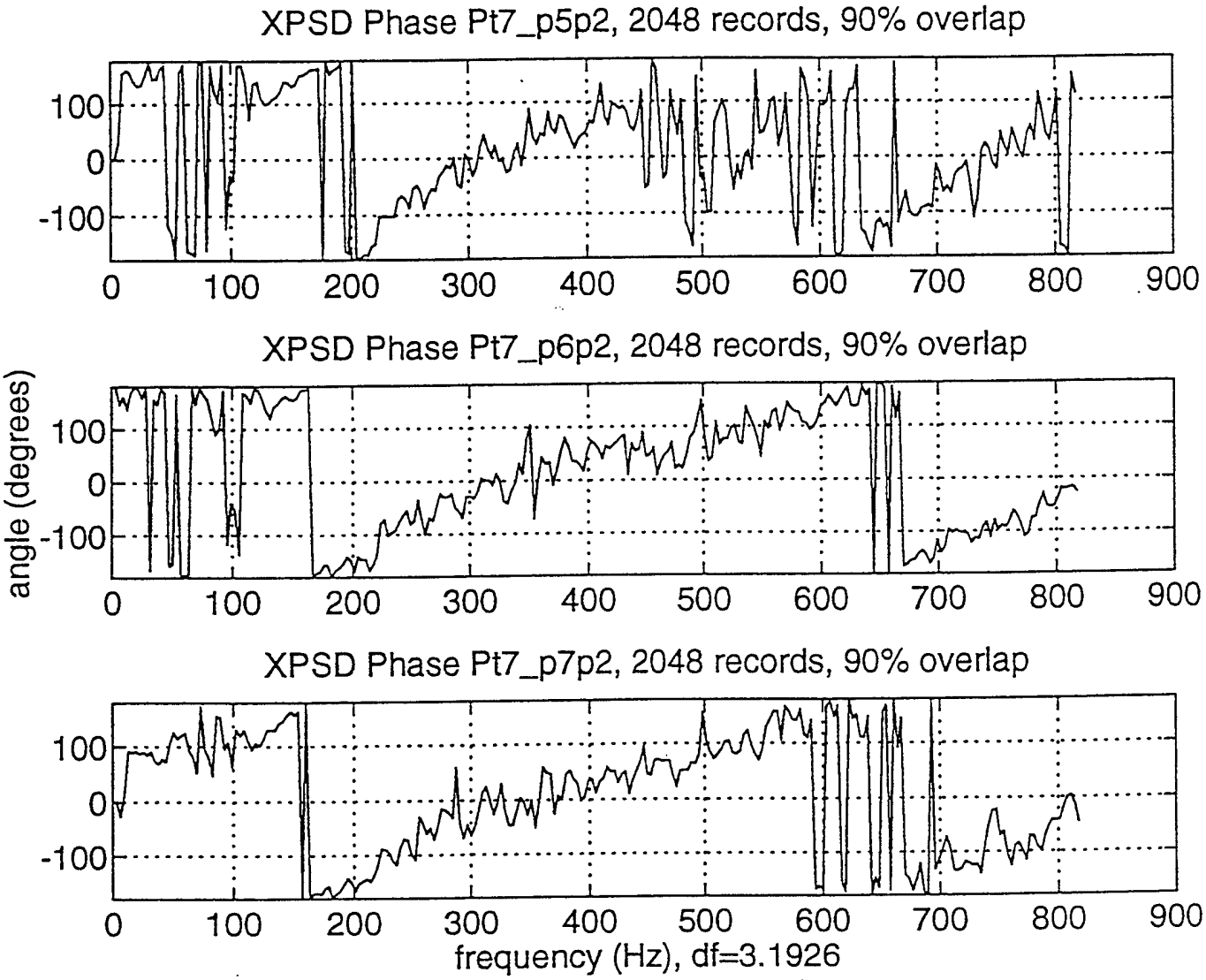

Figure 13. Phase of pressure cross-PSDs relating measurement points 5,6 & 7 to 2.

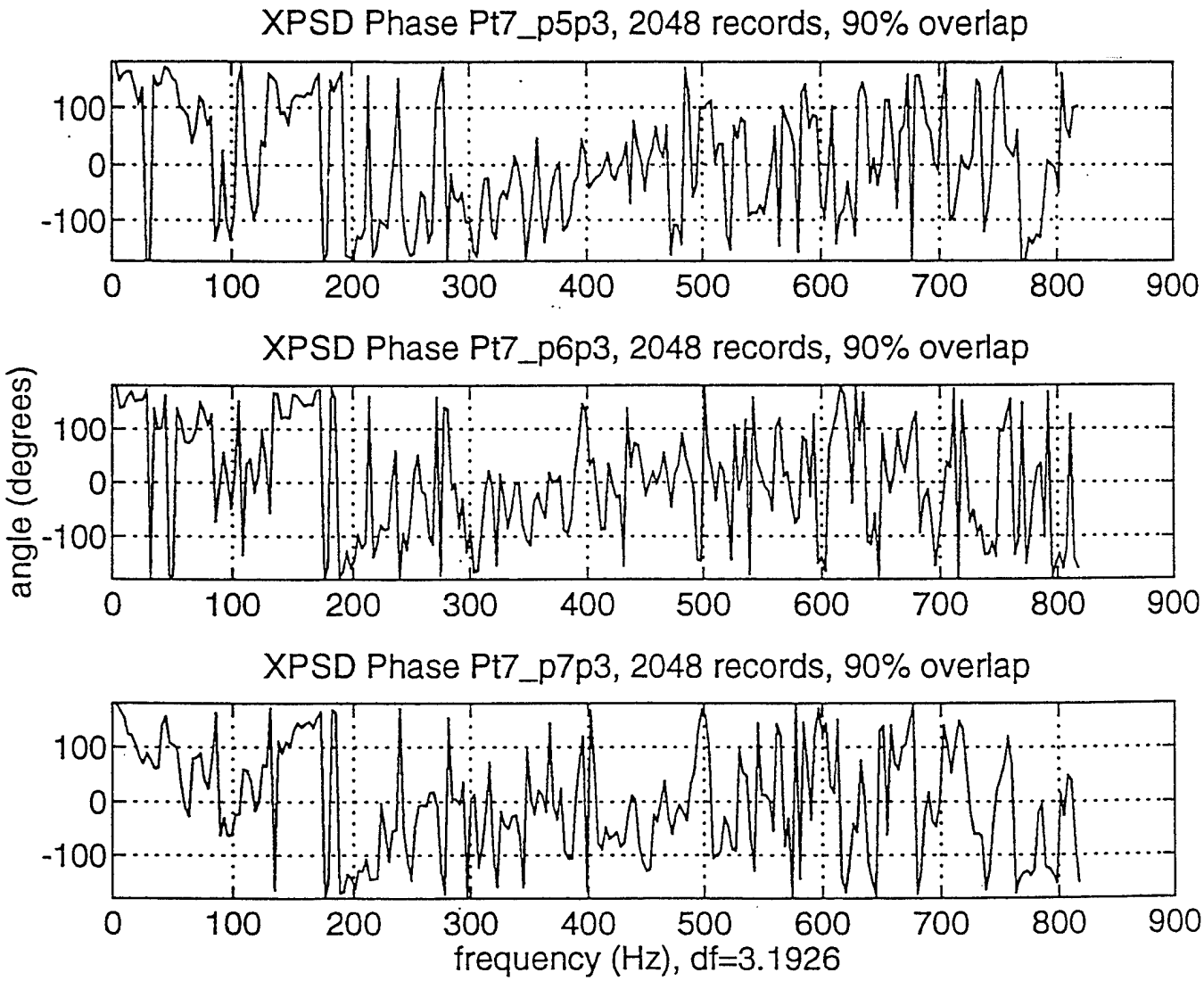

Figure 14. Phase of pressure cross-PSDs relating measurement points 5,6 & 7 to 3.

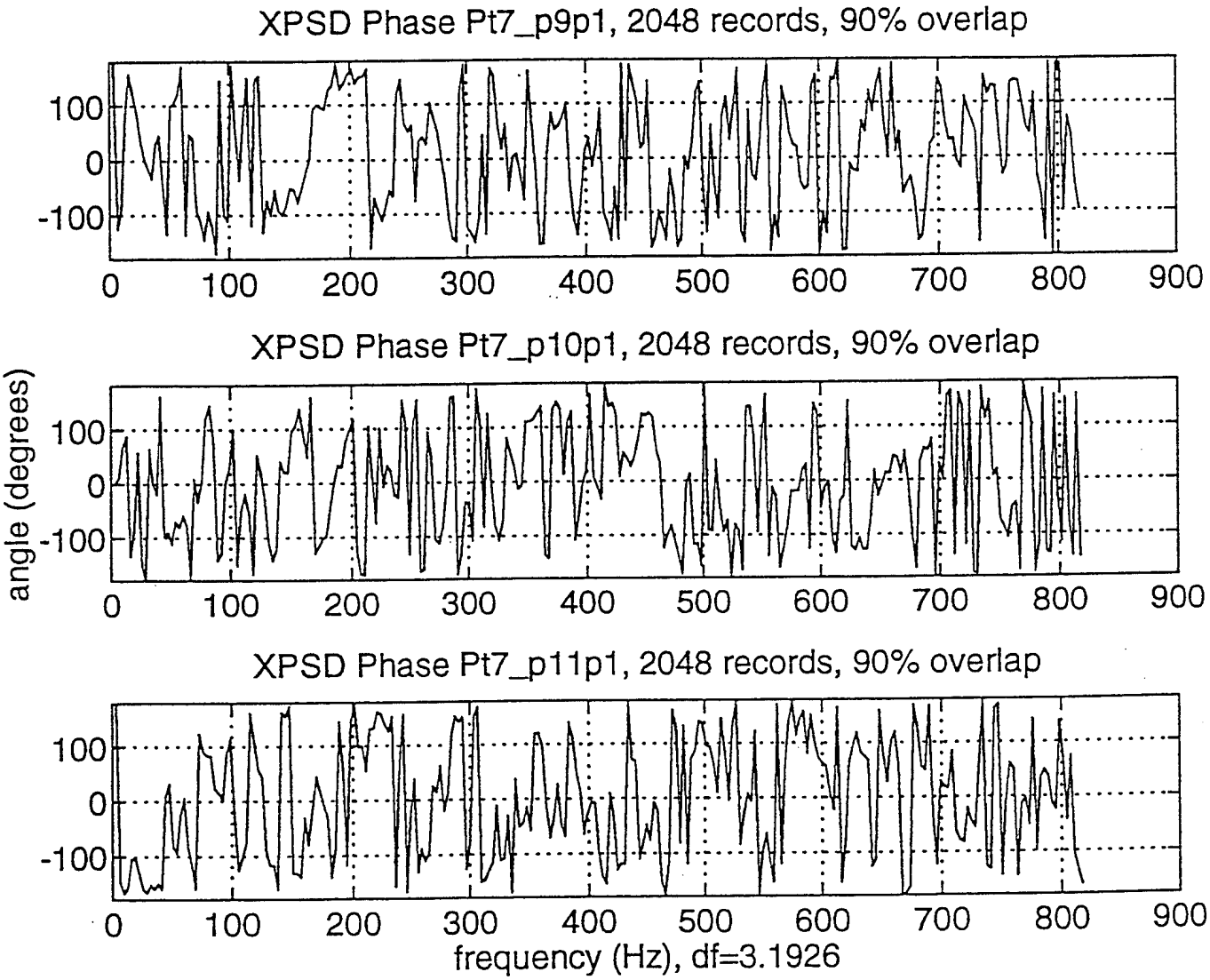

Figure 15. Phase of pressure cross-PSDs relating measurement points 9, 10 & 11 to 1.

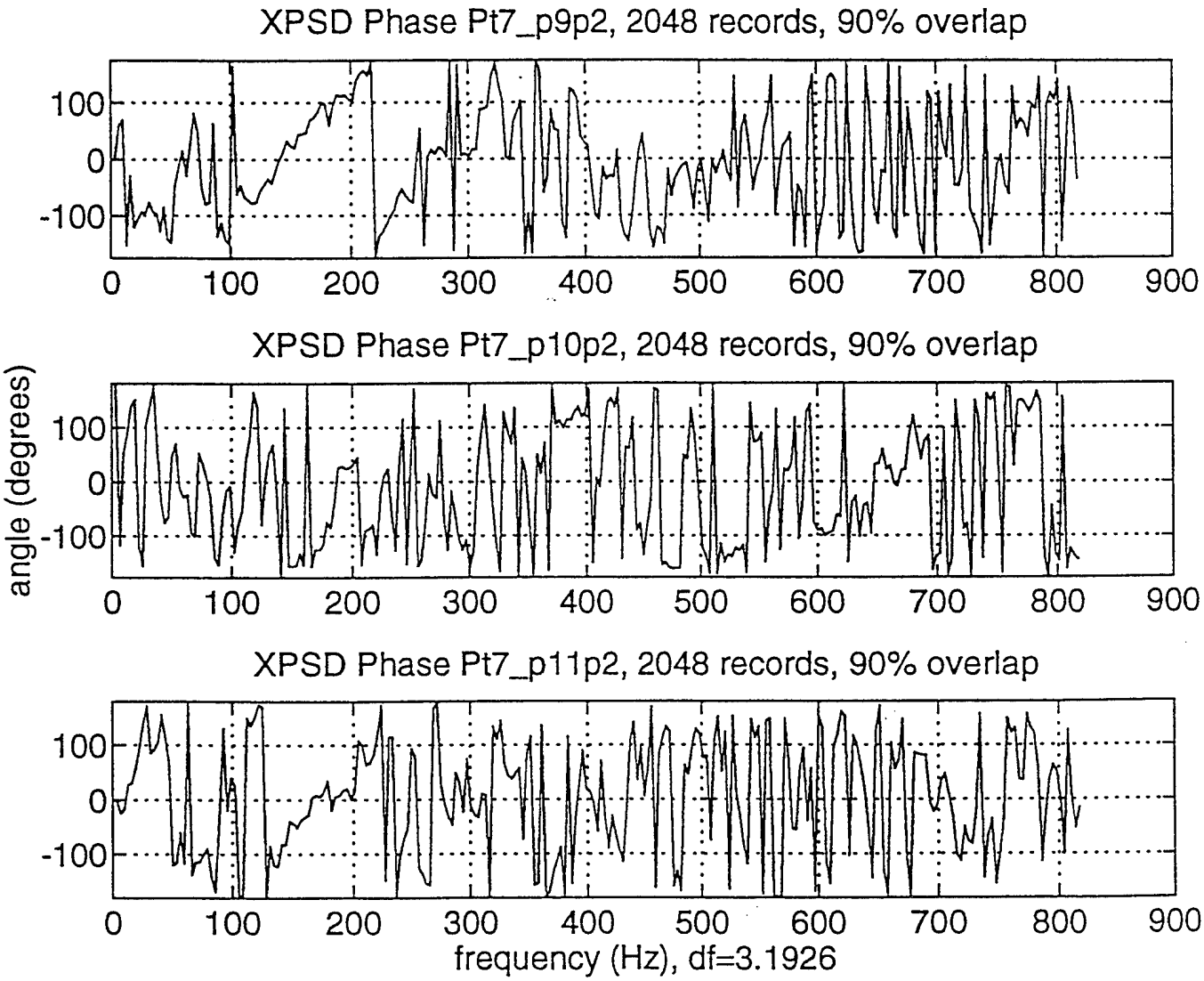

Figure 16. Phase of pressure cross-PSDs relating measurement points 9, 10 & 11 to 2.

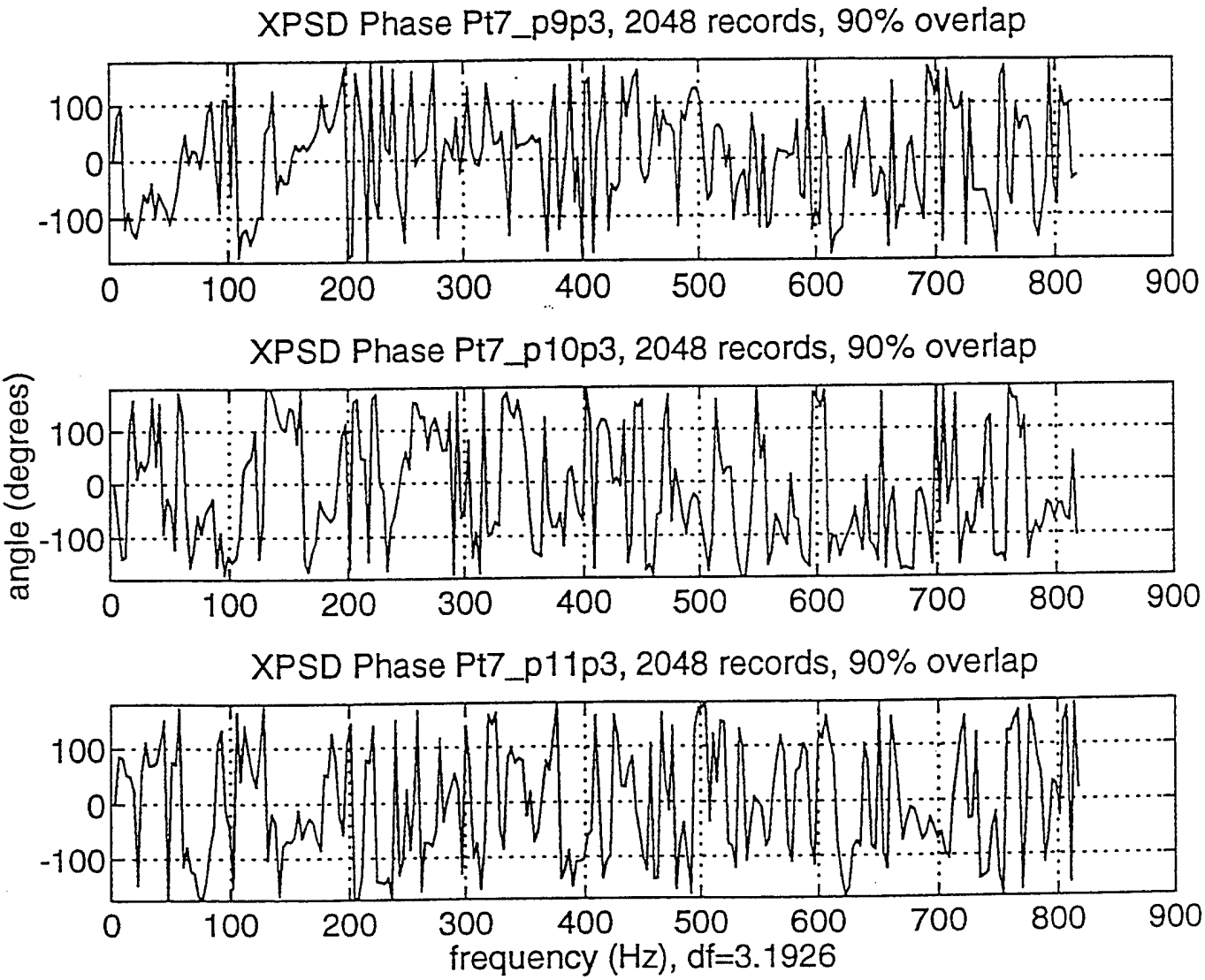

Figure 17. Phase of pressure cross-PSDs relating measurement points 9,10 & 11 to 3.

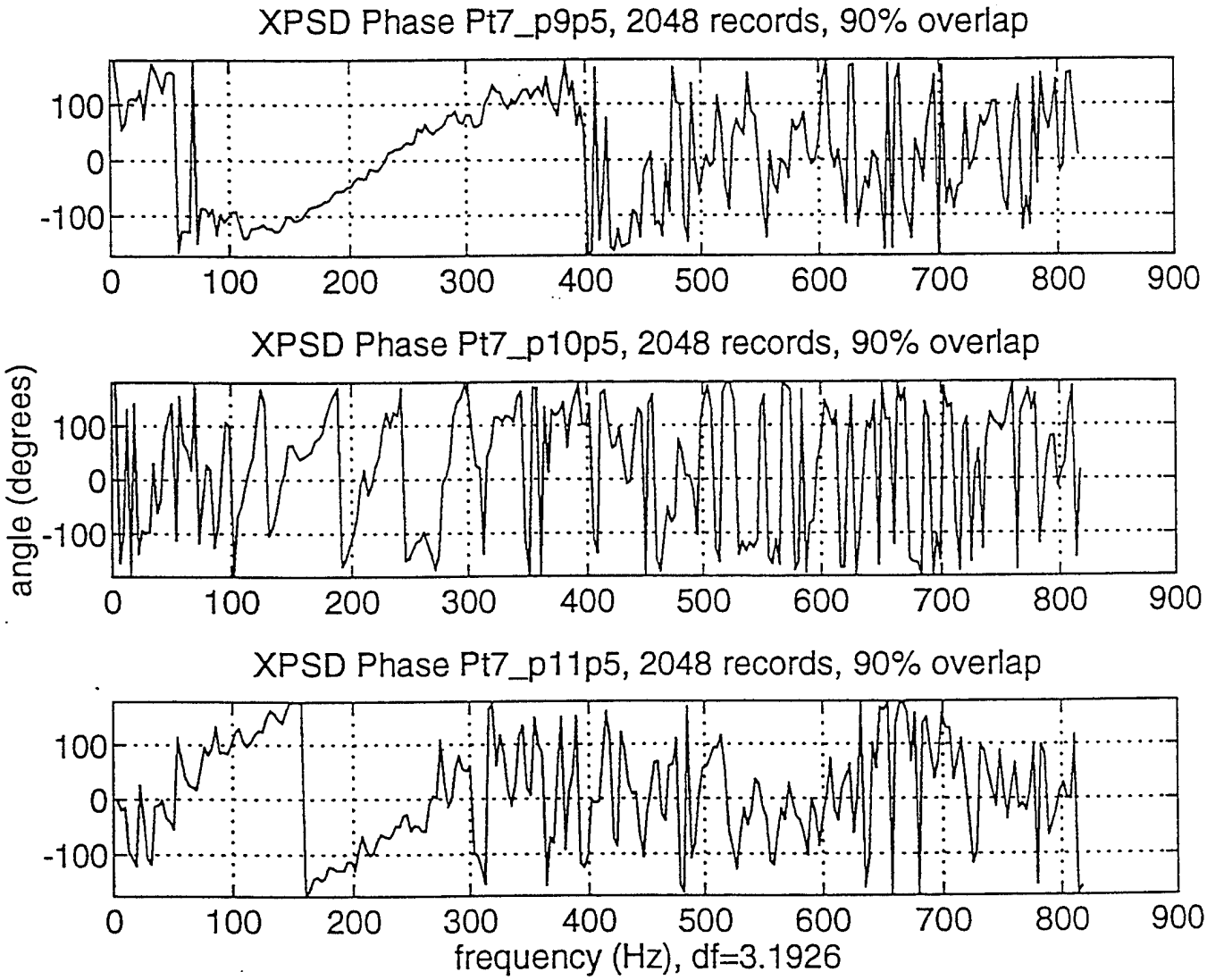

Figure 18. Phase of pressure cross-PSDs relating measurement points 9, 10 & 11 to 5.

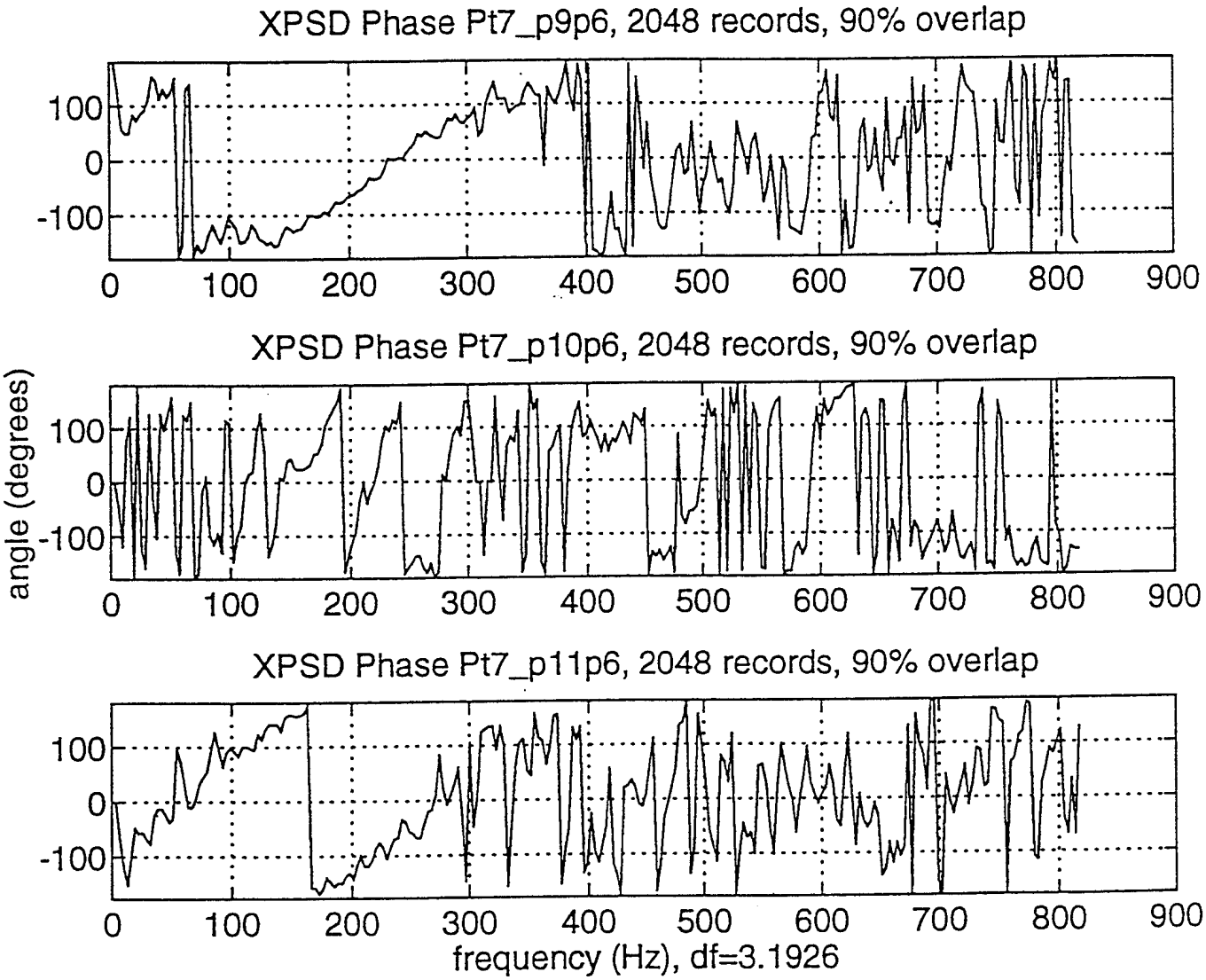

Figure 19. Phase of pressure cross-PSDs relating measurement points 9,10 & 11 to 6.

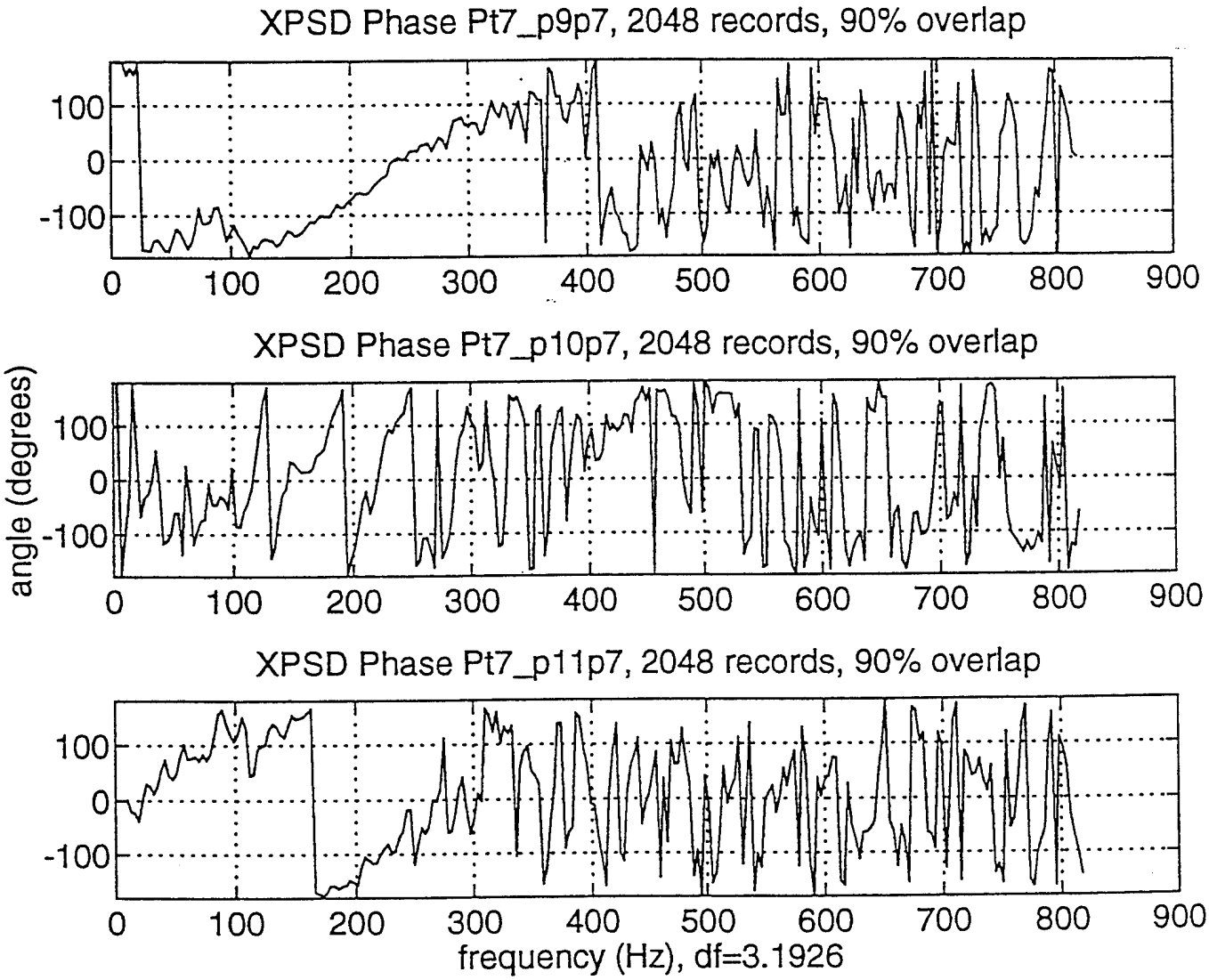

Figure 20. Phase of pressure cross-PSDs relating measurement points 9, 10 & 11 to 7.

Appendix A
Pressure Time Histories

Each plot in this appendix is a pressure (psi) versus time (sec) record. The label for each plot is of the form "Pt7_p*i*", where the *i* indicates the measurement point as shown in Figure 3. [Therefore, *i* ranges from 1 to 17, excluding 4 and 8.]

pt7_p1

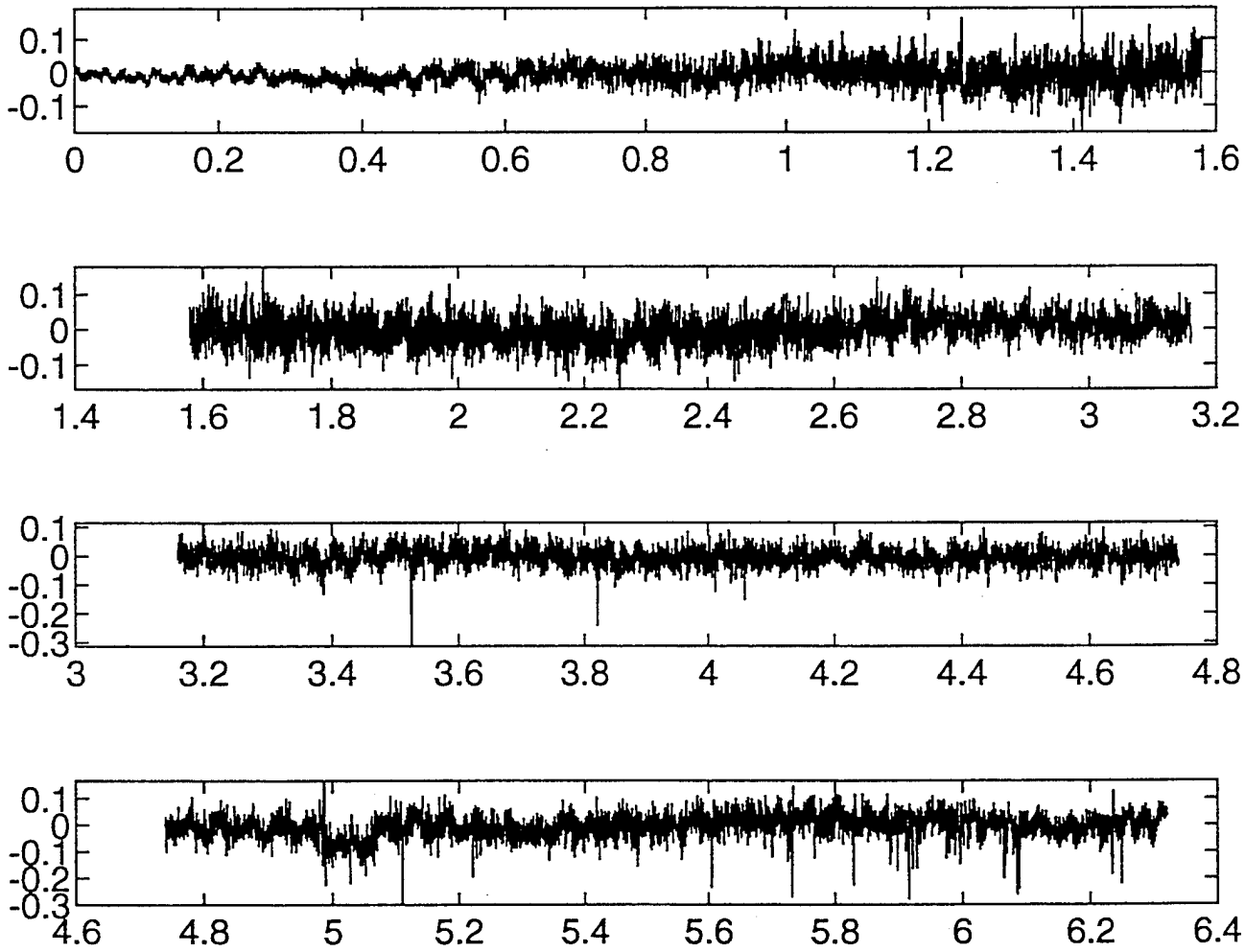
0.1
0
-0.1
0
0.2
0.4
0.6
0.8
1
1.2
1.4
1.6
0.1
0
-0.1
1.4
1.6
1.8
2
2.2
2.4
2.6
2.8
3
3.2
0.1
0
-0.1
-0.2
-0.3
3
3.2
3.4
3.6
3.8
4
4.2
4.4
4.6
4.8
0.1
0
-0.1
-0.2
-0.3
4.6
4.8
5
5.2
5.4
5.6
5.8
6
6.2
6.4

P+7_P2

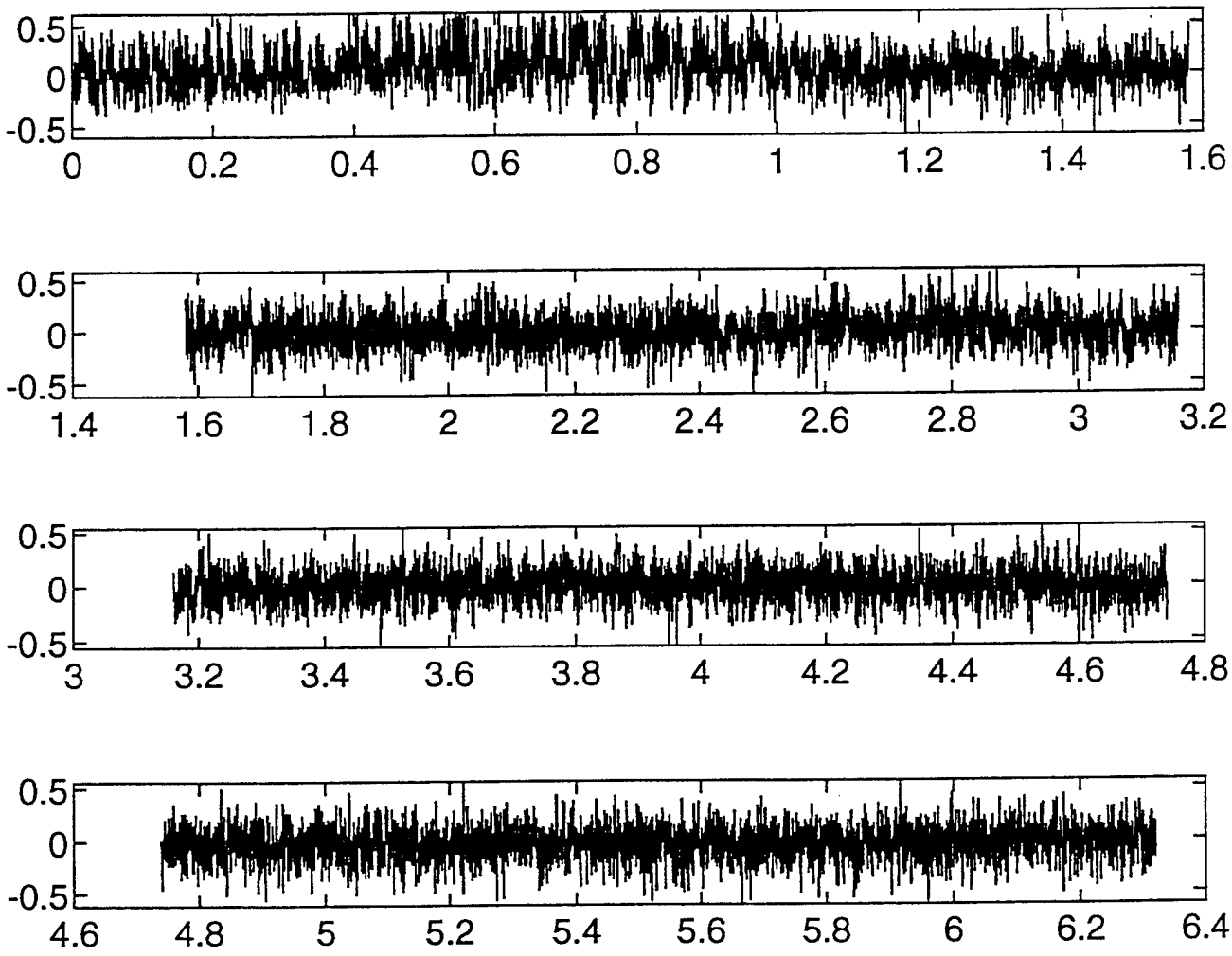
0.5
0
-0.5
0 0.2 0.4 0.6 0.8 1 1.2 1.4 1.6
0.5
0
-0.5
1.4 1.6 1.8 2 2.2 2.4 2.6 2.8 3 3.2
0.5
0
-0.5
3 3.2 3.4 3.6 3.8 4 4.2 4.4 4.6 4.8
0.5
0
-0.5
4.6 4.8 5 5.2 5.4 5.6 5.8 6 6.2 6.4

pt7_p3

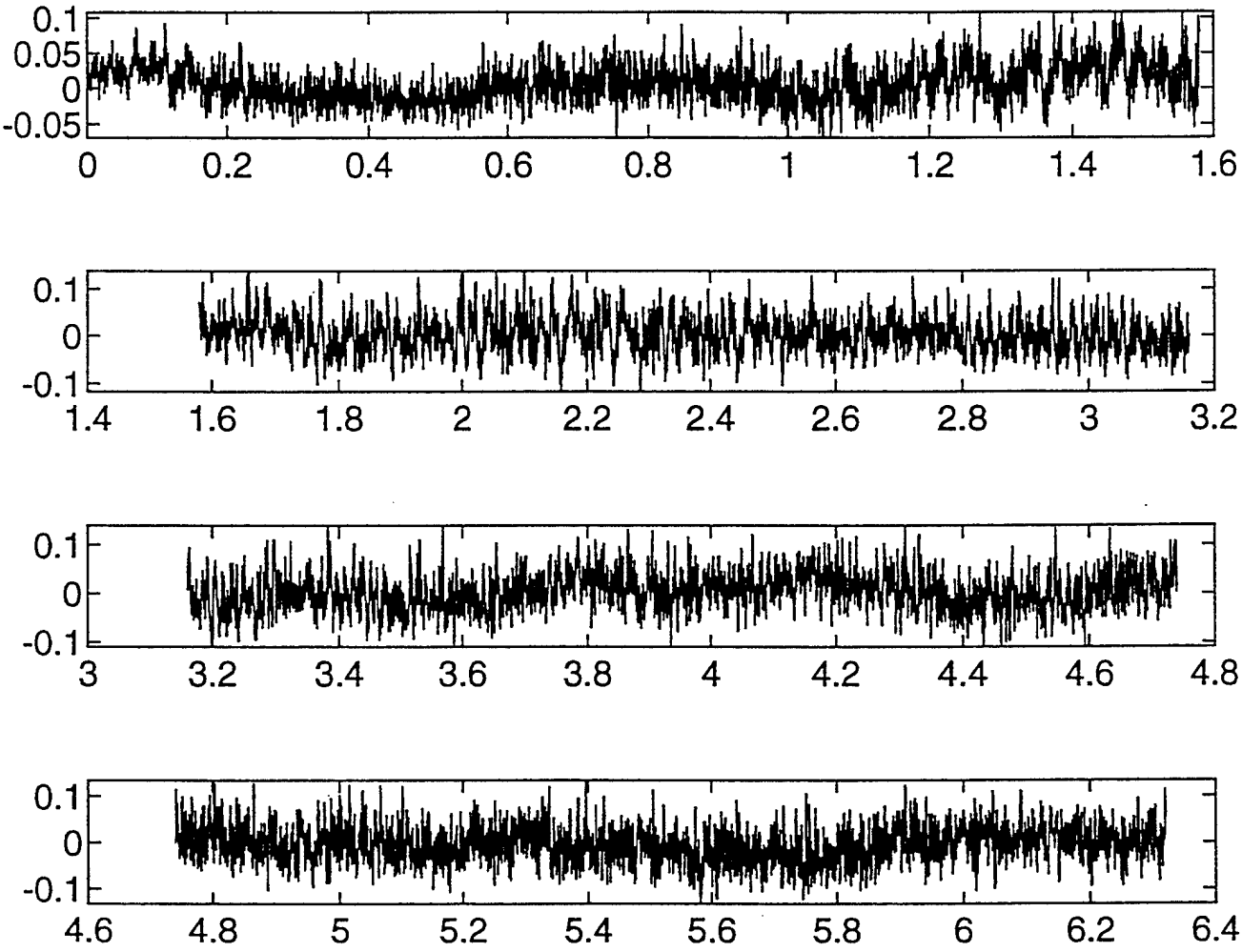
0.1
0.05
0
-0.05
0 0.2 0.4 0.6 0.8 1 1.2 1.4 1.6
0.1
0
-0.1
1.4 1.6 1.8 2 2.2 2.4 2.6 2.8 3 3.2
0.1
0
-0.1
3 3.2 3.4 3.6 3.8 4 4.2 4.4 4.6 4.8
0.1
0
-0.1
4.6 4.8 5 5.2 5.4 5.6 5.8 6 6.2 6.4

pt7_p5

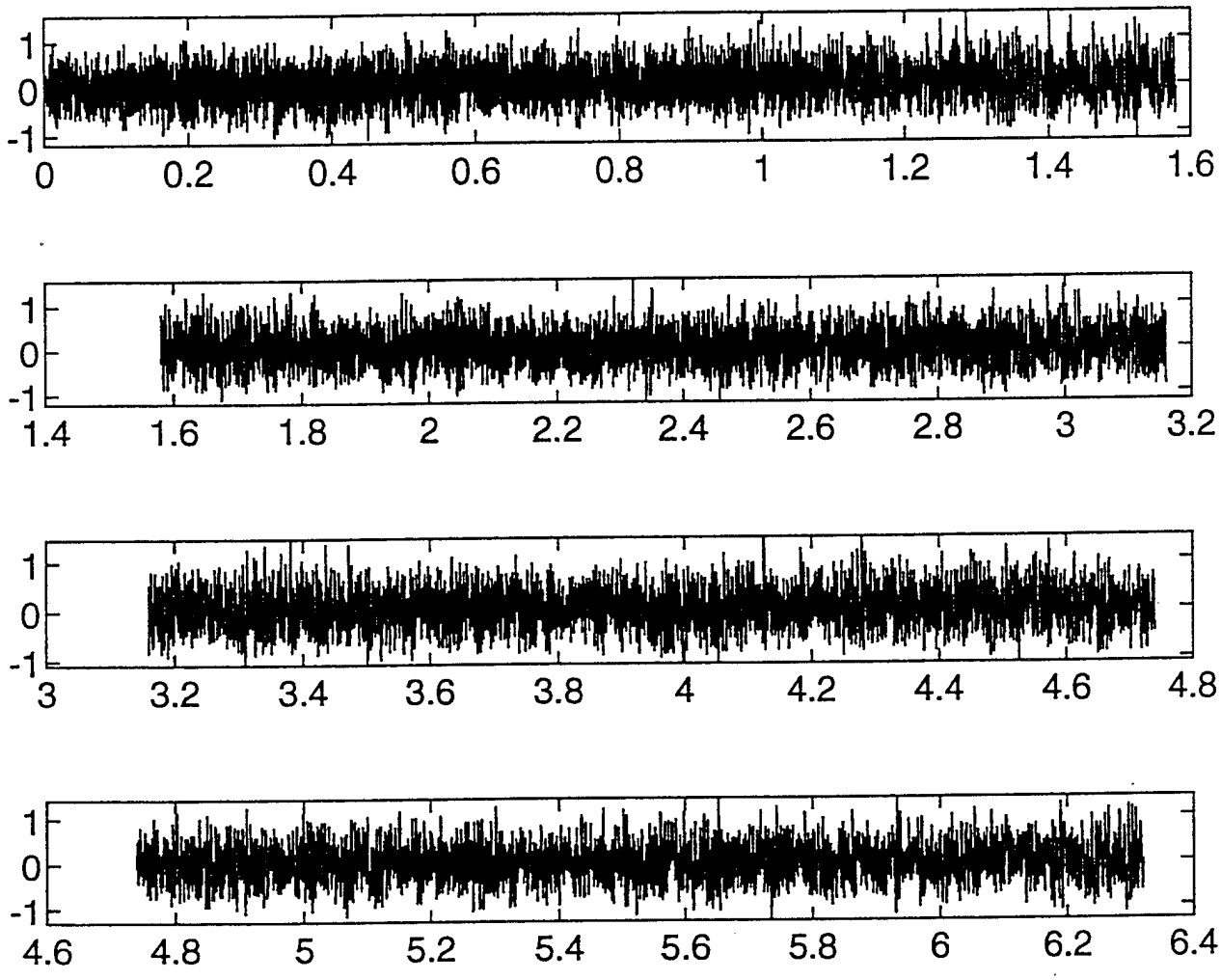
1
0
-1
0 0.2 0.4 0.6 0.8 1 1.2 1.4 1.6
1
0
-1
1.4 1.6 1.8 2 2.2 2.4 2.6 2.8 3 3.2
1
0
-1
3 3.2 3.4 3.6 3.8 4 4.2 4.4 4.6 4.8
1
0
-1
4.6 4.8 5 5.2 5.4 5.6 5.8 6 6.2 6.4

p47_p6

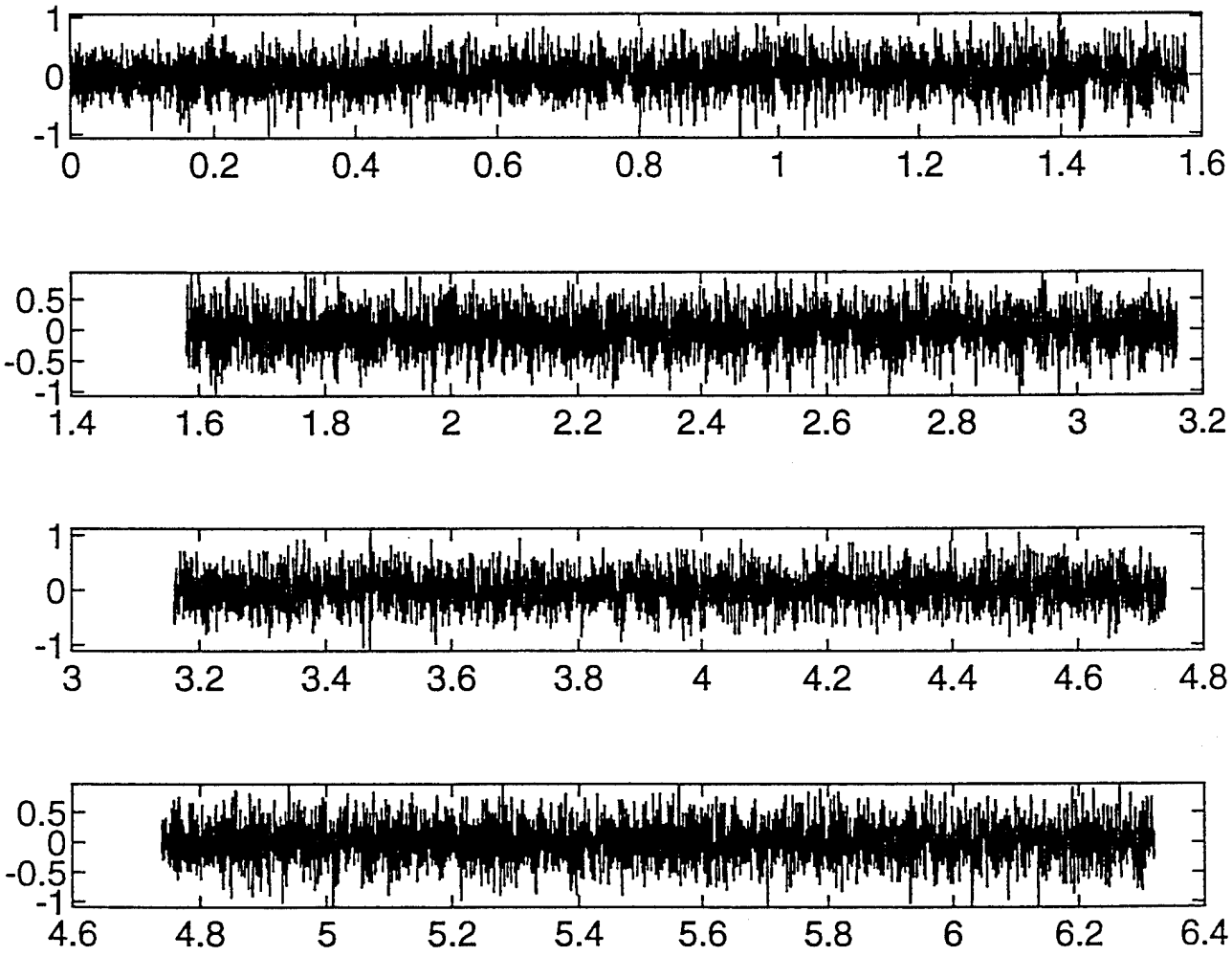
1
0
-1
0 0.2 0.4 0.6 0.8 1 1.2 1.4 1.6
0.5
0
-0.5
-1
1.4 1.6 1.8 2 2.2 2.4 2.6 2.8 3 3.2
1
0
-1
3 3.2 3.4 3.6 3.8 4 4.2 4.4 4.6 4.8
0.5
0
-0.5
-1
4.6 4.8 5 5.2 5.4 5.6 5.8 6 6.2 6.4

p47_p7

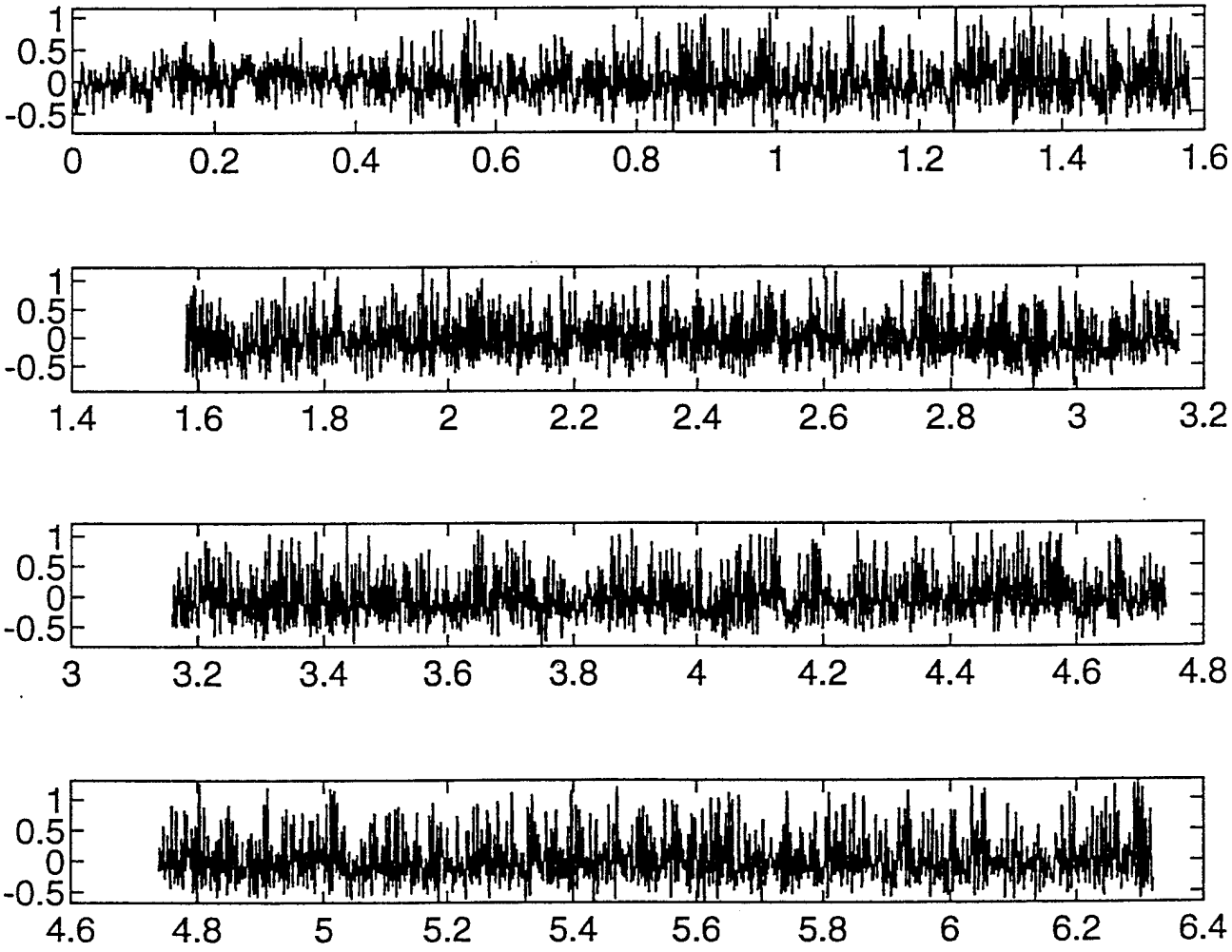
1
0.5
0
-0.5
0 0.2 0.4 0.6 0.8 1 1.2 1.4 1.6
1.4 1.6 1.8 2 2.2 2.4 2.6 2.8 3 3.2
3 3.2 3.4 3.6 3.8 4 4.2 4.4 4.6 4.8
4.6 4.8 5 5.2 5.4 5.6 5.8 6 6.2 6.4

P+7_P9

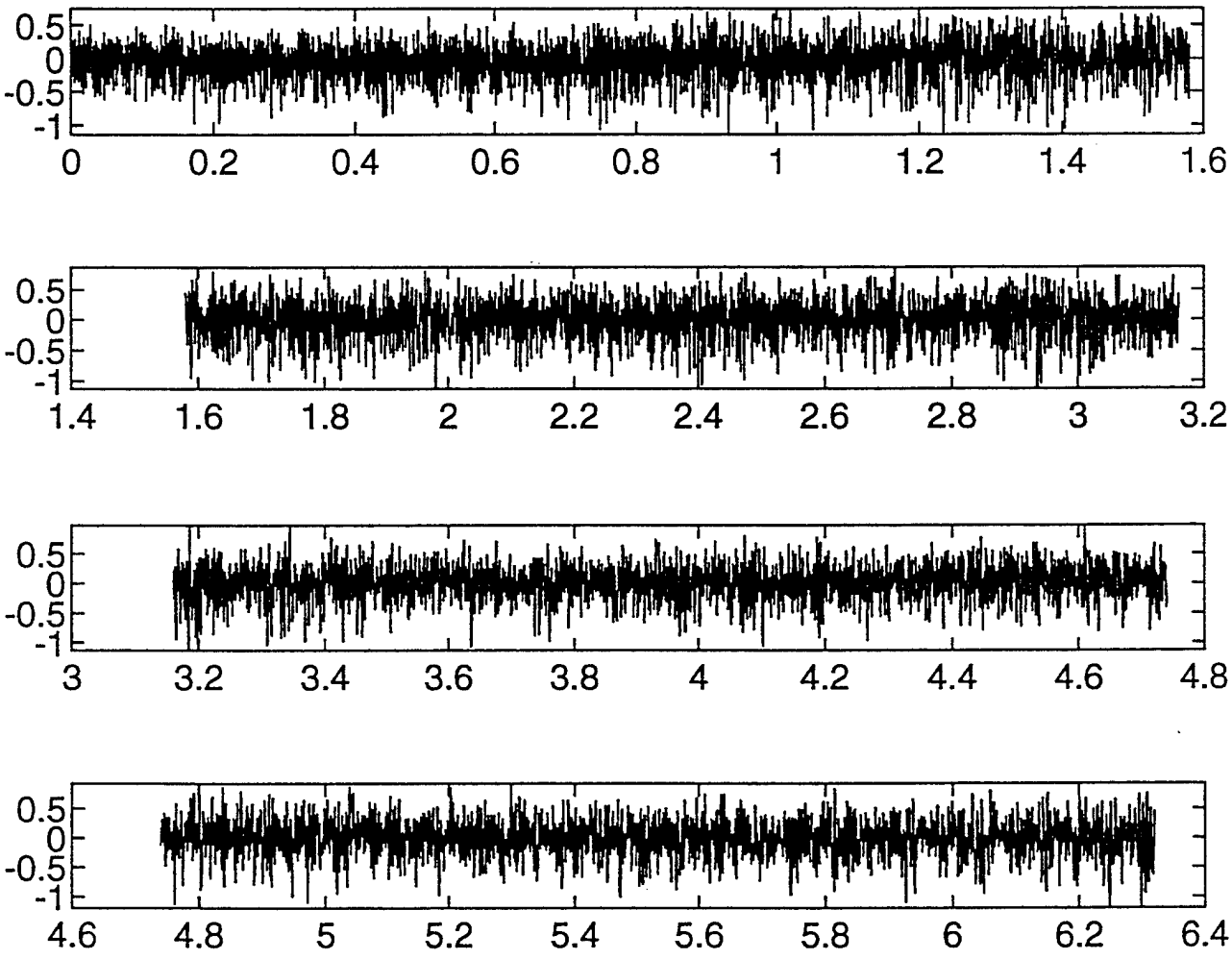
0.5
0
-0.5
-1
0 0.2 0.4 0.6 0.8 1 1.2 1.4 1.6
0.5
0
-0.5
-1
1.4 1.6 1.8 2 2.2 2.4 2.6 2.8 3 3.2
0.5
0
-0.5
-1
3 3.2 3.4 3.6 3.8 4 4.2 4.4 4.6 4.8
0.5
0
-0.5
-1
4.6 4.8 5 5.2 5.4 5.6 5.8 6 6.2 6.4

p+7-p10

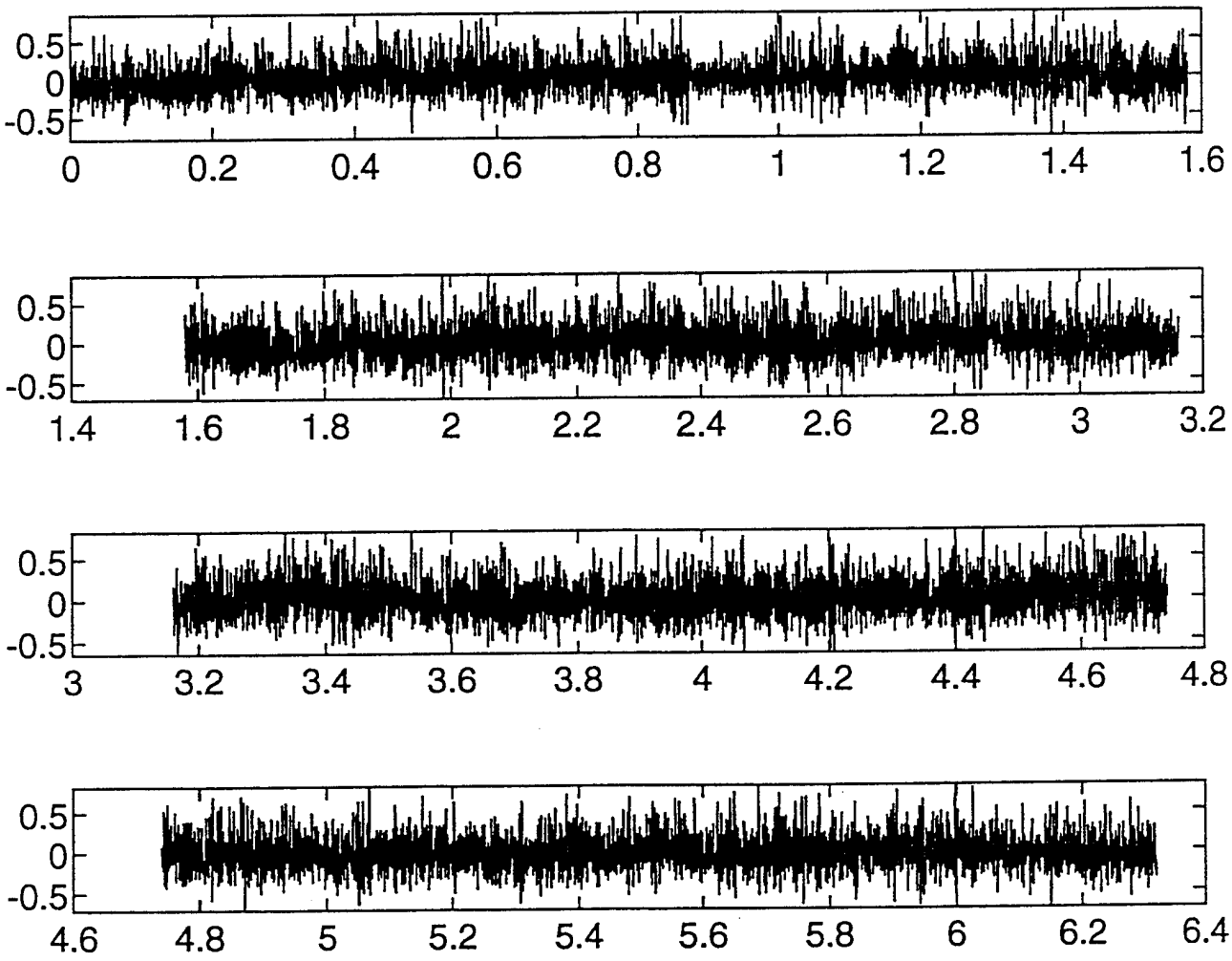
0.5
0
-0.5
0 0.2 0.4 0.6 0.8 1 1.2 1.4 1.6
0.5
0
-0.5
1.4 1.6 1.8 2 2.2 2.4 2.6 2.8 3 3.2
0.5
0
-0.5
3 3.2 3.4 3.6 3.8 4 4.2 4.4 4.6 4.8
0.5
0
-0.5
4.6 4.8 5 5.2 5.4 5.6 5.8 6 6.2 6.4

P+7_p 11

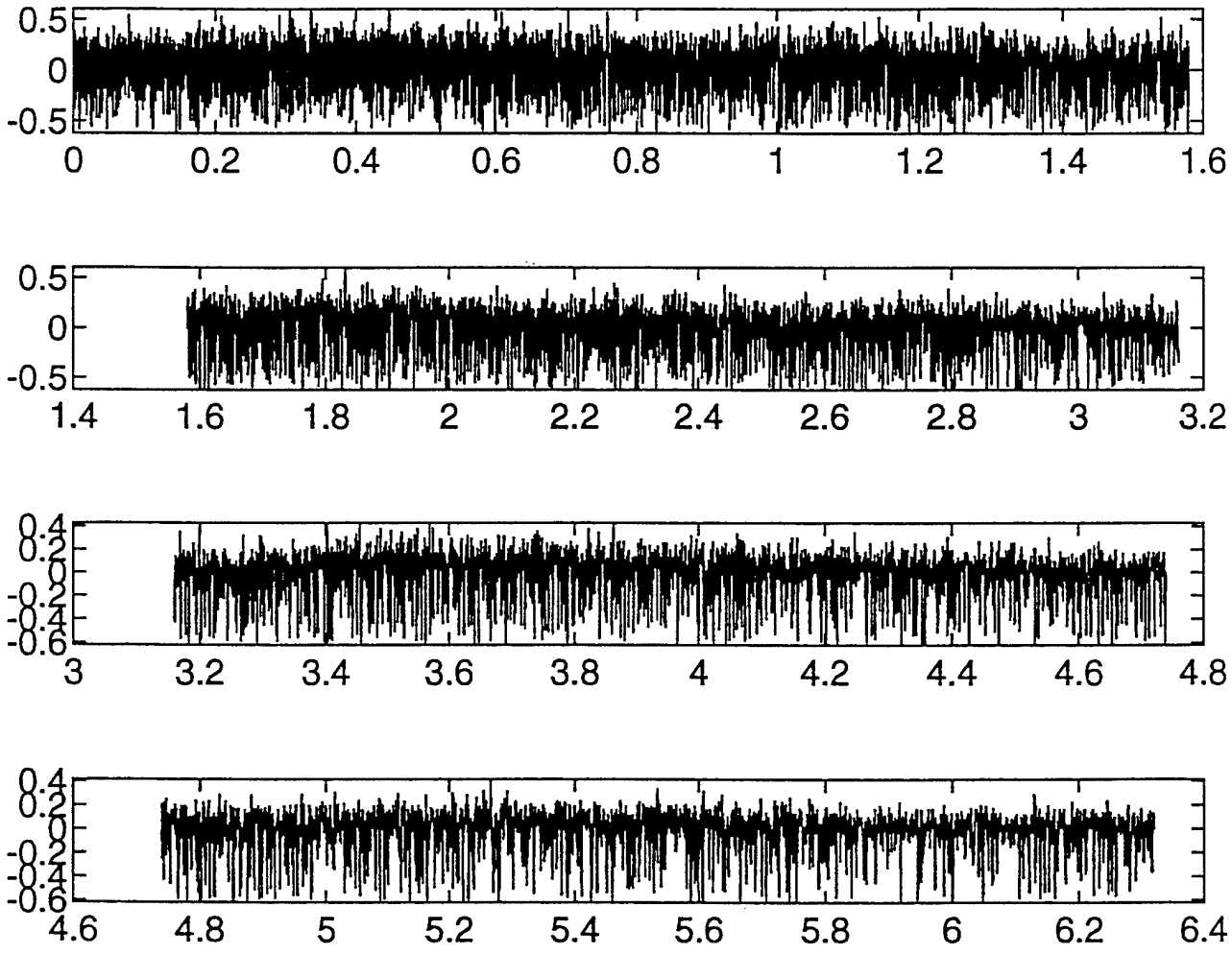
0.5
0
-0.5
0 0.2 0.4 0.6 0.8 1 1.2 1.4 1.6
0.5
0
-0.5
1.4 1.6 1.8 2 2.2 2.4 2.6 2.8 3 3.2
0.4
0.2
0
-0.2
-0.4
-0.6
3 3.2 3.4 3.6 3.8 4 4.2 4.4 4.6 4.8
0.4
0.2
0
-0.2
-0.4
-0.6
4.6 4.8 5 5.2 5.4 5.6 5.8 6 6.2 6.4

p47_p12

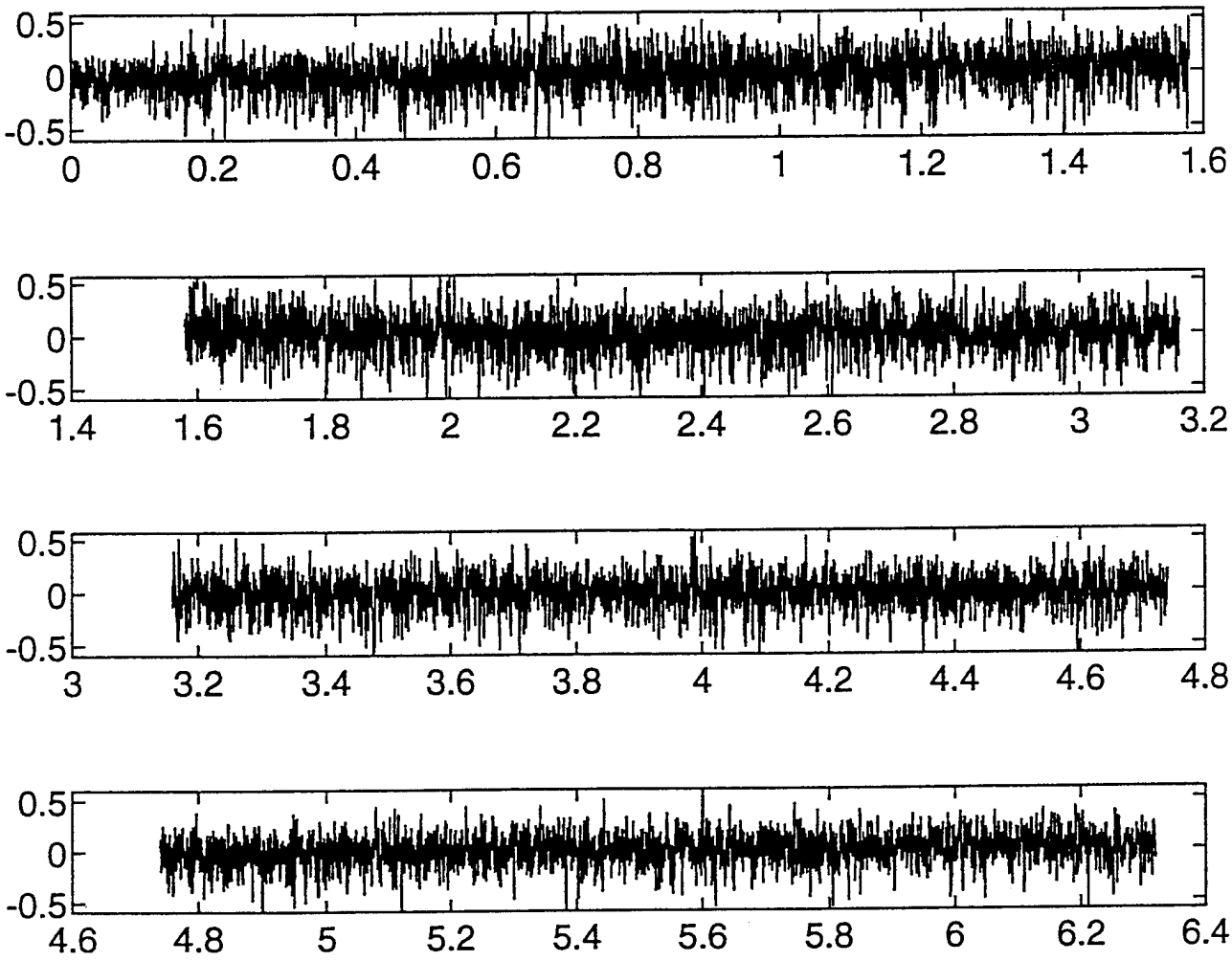
0.5
0
-0.5
0 0.2 0.4 0.6 0.8 1 1.2 1.4 1.6
0.5
0
-0.5
1.4 1.6 1.8 2 2.2 2.4 2.6 2.8 3 3.2
0.5
0
-0.5
3 3.2 3.4 3.6 3.8 4 4.2 4.4 4.6 4.8
0.5
0
-0.5
4.6 4.8 5 5.2 5.4 5.6 5.8 6 6.2 6.4

pf7_p13

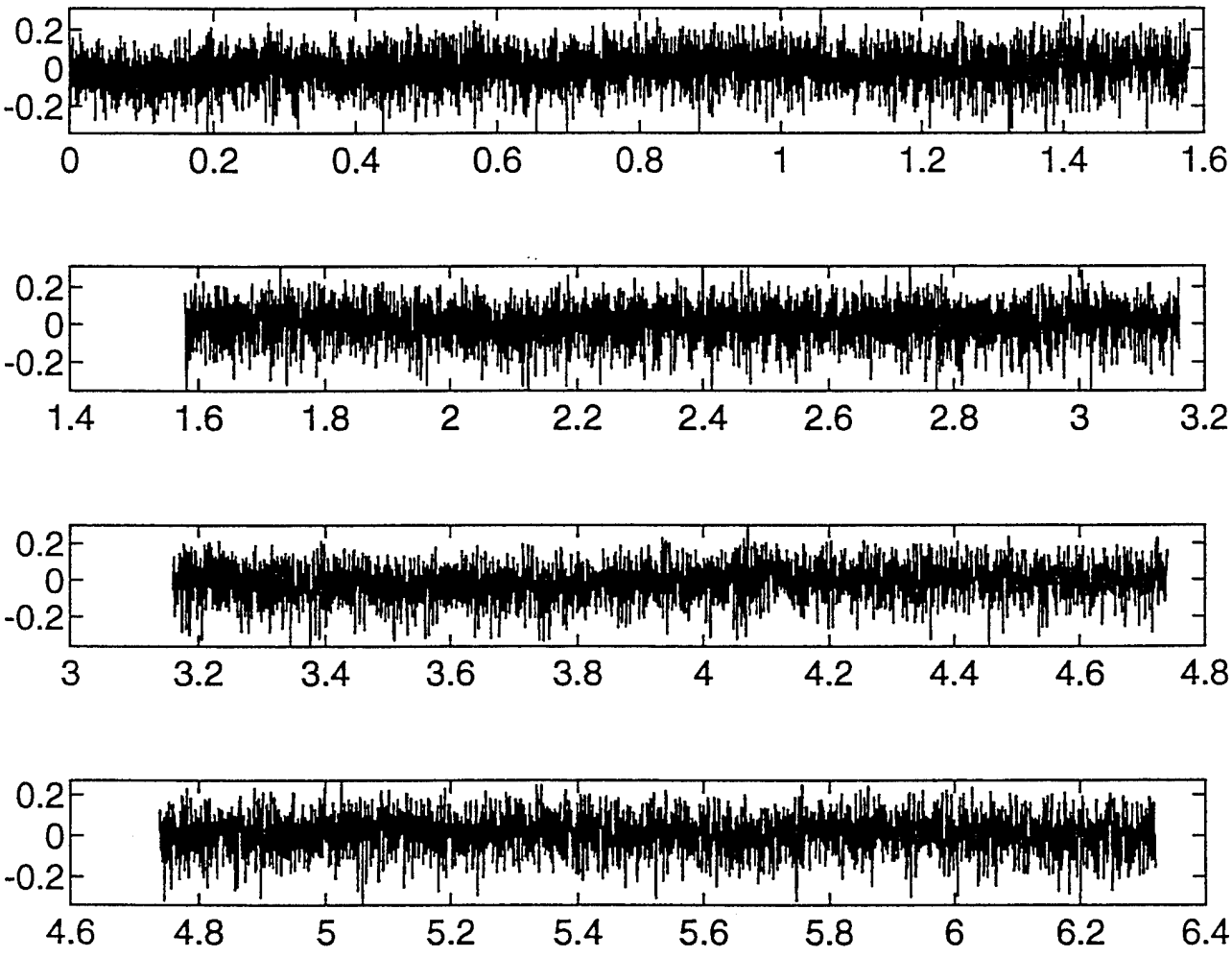
0.2
0
-0.2
0 0.2 0.4 0.6 0.8 1 1.2 1.4 1.6
0.2
0
-0.2
1.4 1.6 1.8 2 2.2 2.4 2.6 2.8 3 3.2
0.2
0
-0.2
3 3.2 3.4 3.6 3.8 4 4.2 4.4 4.6 4.8
0.2
0
-0.2
4.6 4.8 5 5.2 5.4 5.6 5.8 6 6.2 6.4

p17 - p14

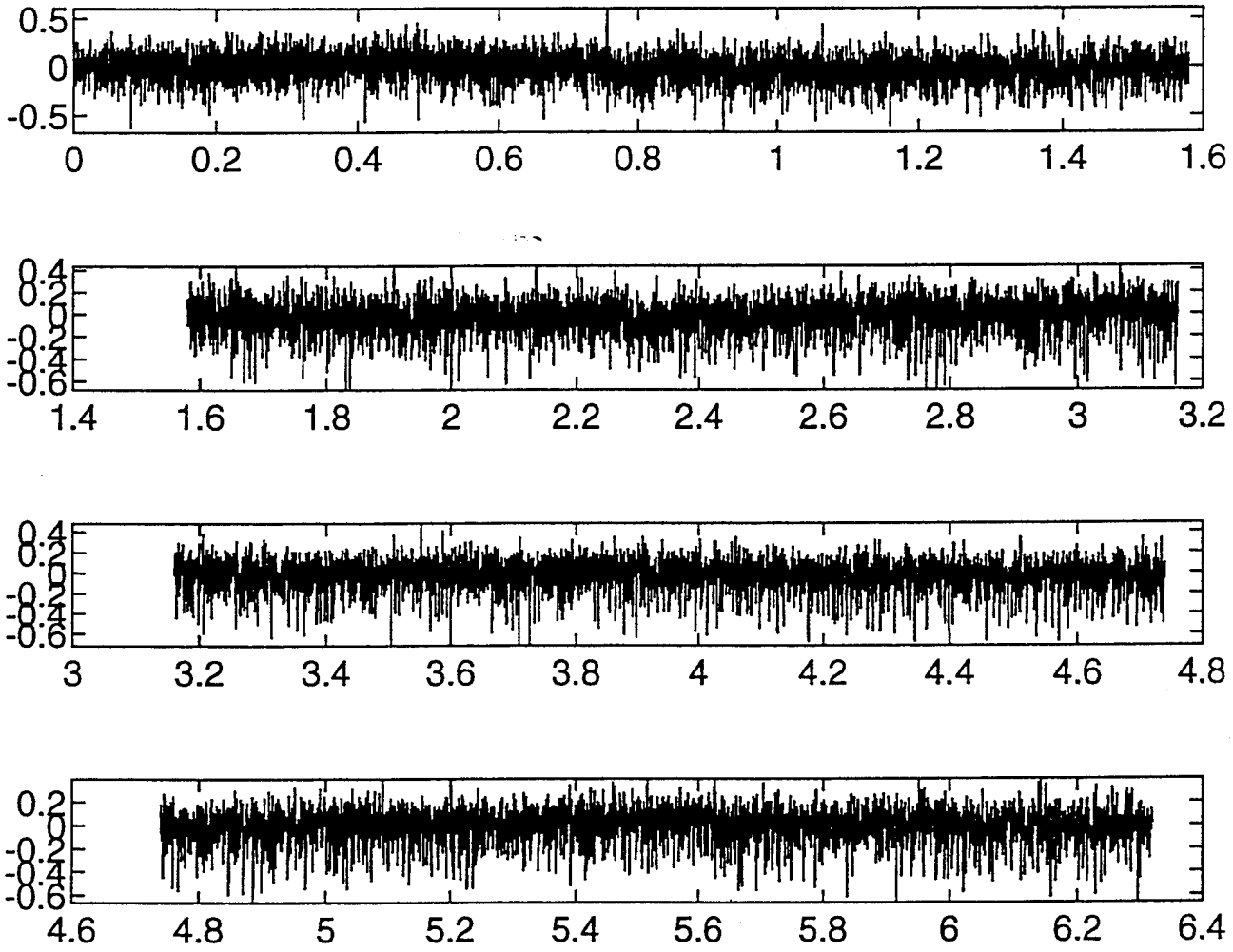
0.5
0
-0.5
0 0.2 0.4 0.6 0.8 1 1.2 1.4 1.6
0.4
0.2
0
-0.2
-0.4
-0.6
1.4 1.6 1.8 2 2.2 2.4 2.6 2.8 3 3.2
0.4
0.2
0
-0.2
-0.4
-0.6
3 3.2 3.4 3.6 3.8 4 4.2 4.4 4.6 4.8
0.2
0
-0.2
-0.4
-0.6
4.6 4.8 5 5.2 5.4 5.6 5.8 6 6.2 6.4

pt7-pt5

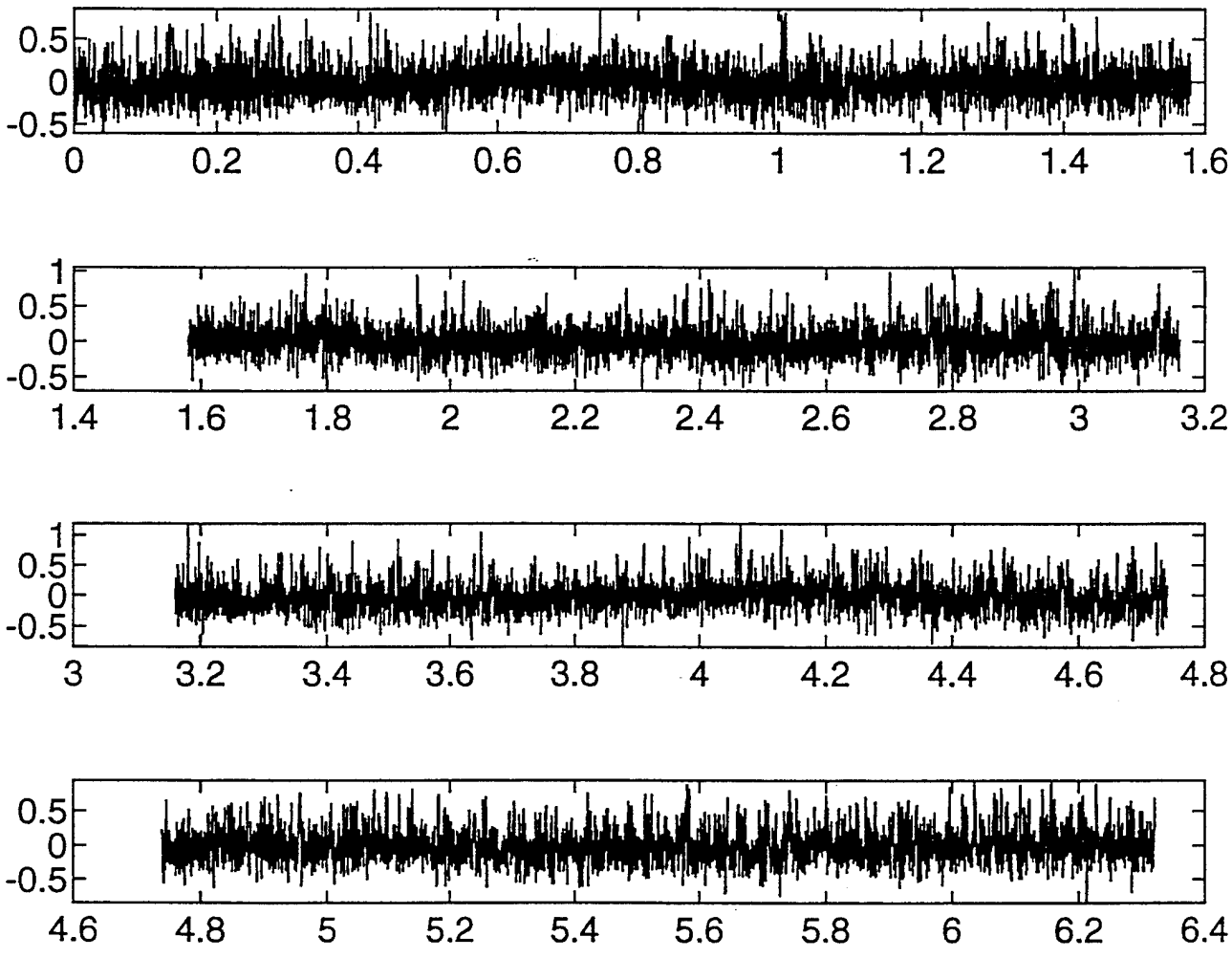
0.5
0
-0.5
0
0.2
0.4
0.6
0.8
1
1.2
1.4
1.6
1
0.5
0
-0.5
1.4
1.6
1.8
2
2.2
2.4
2.6
2.8
3
3.2
1
0.5
0
-0.5
3
3.2
3.4
3.6
3.8
4
4.2
4.4
4.6
4.8
0.5
0
-0.5
4.6
4.8
5
5.2
5.4
5.6
5.8
6
6.2
6.4

pft-p16

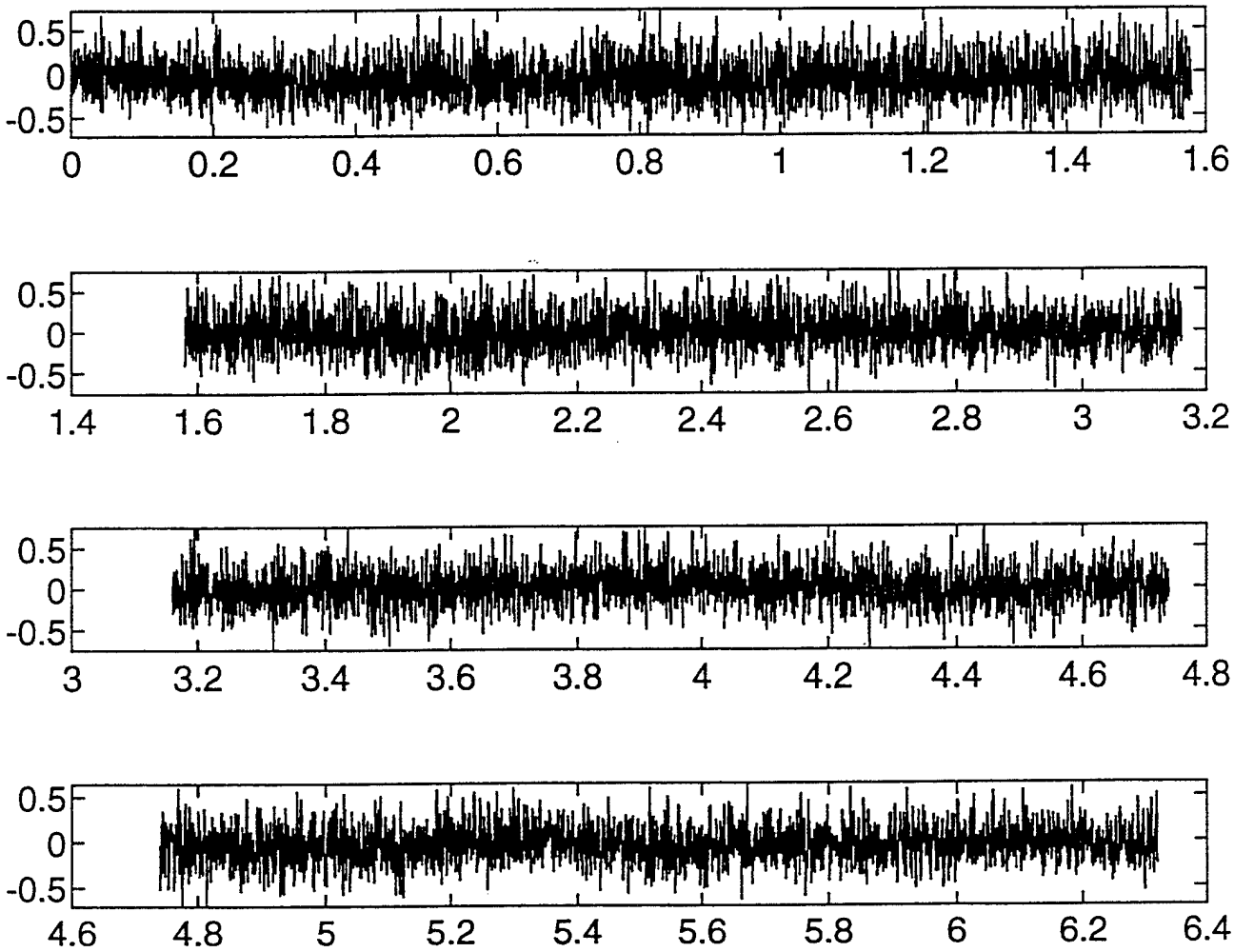
0.5
0
-0.5
0 0.2 0.4 0.6 0.8 1 1.2 1.4 1.6
0.5
0
-0.5
1.4 1.6 1.8 2 2.2 2.4 2.6 2.8 3 3.2
0.5
0
-0.5
3 3.2 3.4 3.6 3.8 4 4.2 4.4 4.6 4.8
0.5
0
-0.5
4.6 4.8 5 5.2 5.4 5.6 5.8 6 6.2 6.4

pt 7_p 17

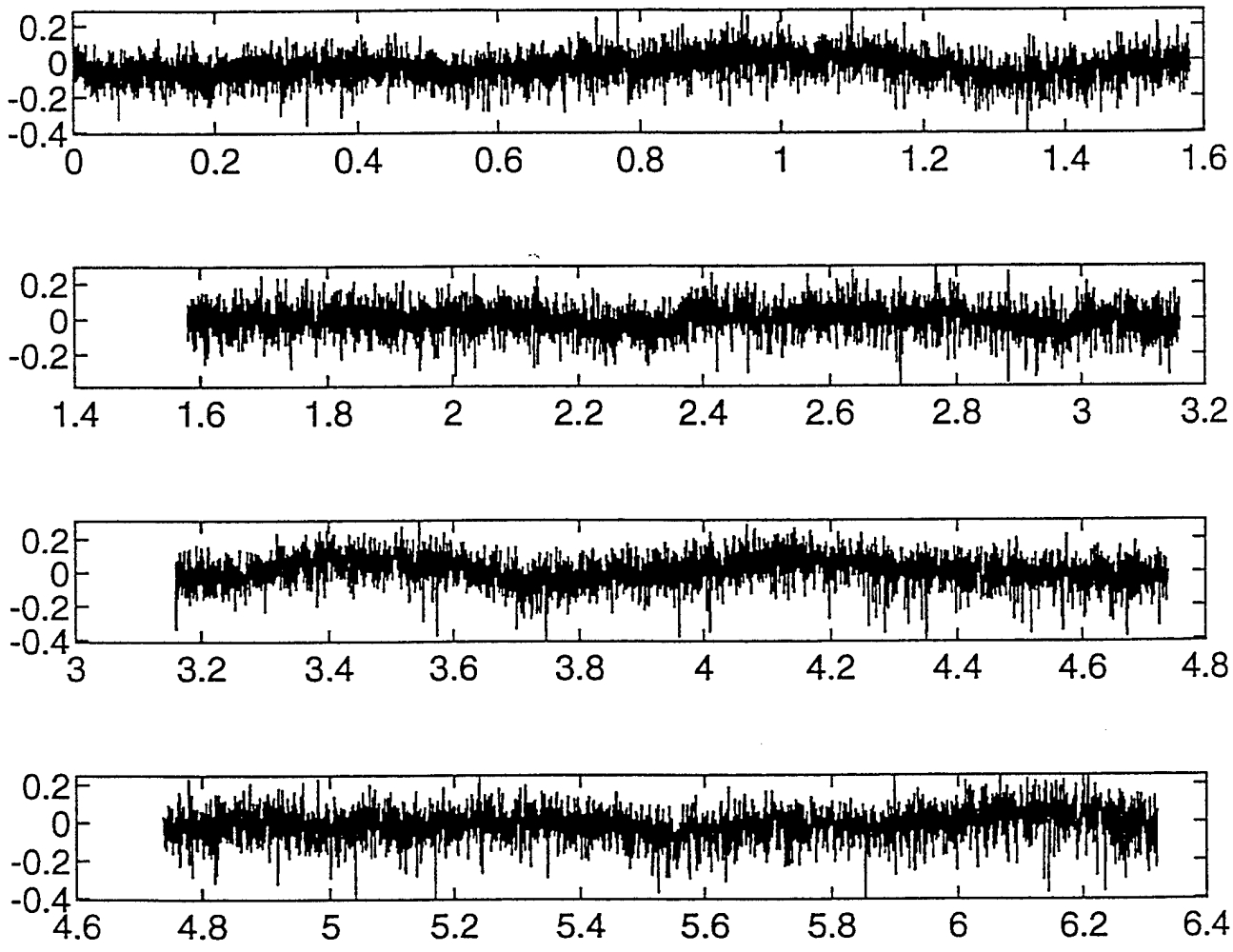
0.2
0
-0.2
-0.4
0 0.2 0.4 0.6 0.8 1 1.2 1.4 1.6
0.2
0
-0.2
1.4 1.6 1.8 2 2.2 2.4 2.6 2.8 3 3.2
0.2
0
-0.2
-0.4
3 3.2 3.4 3.6 3.8 4 4.2 4.4 4.6 4.8
0.2
0
-0.2
-0.4
4.6 4.8 5 5.2 5.4 5.6 5.8 6 6.2 6.4

Appendix B
Pressure Auto-PSDs

Each plot in this appendix is an auto-power spectral density. The label for each plot is of the form "Pt7_p*i*", where the *i* indicates the measurement point as shown in Figure 3. [Therefore, *i* ranges from 1 to 17, excluding 4 and 8.]

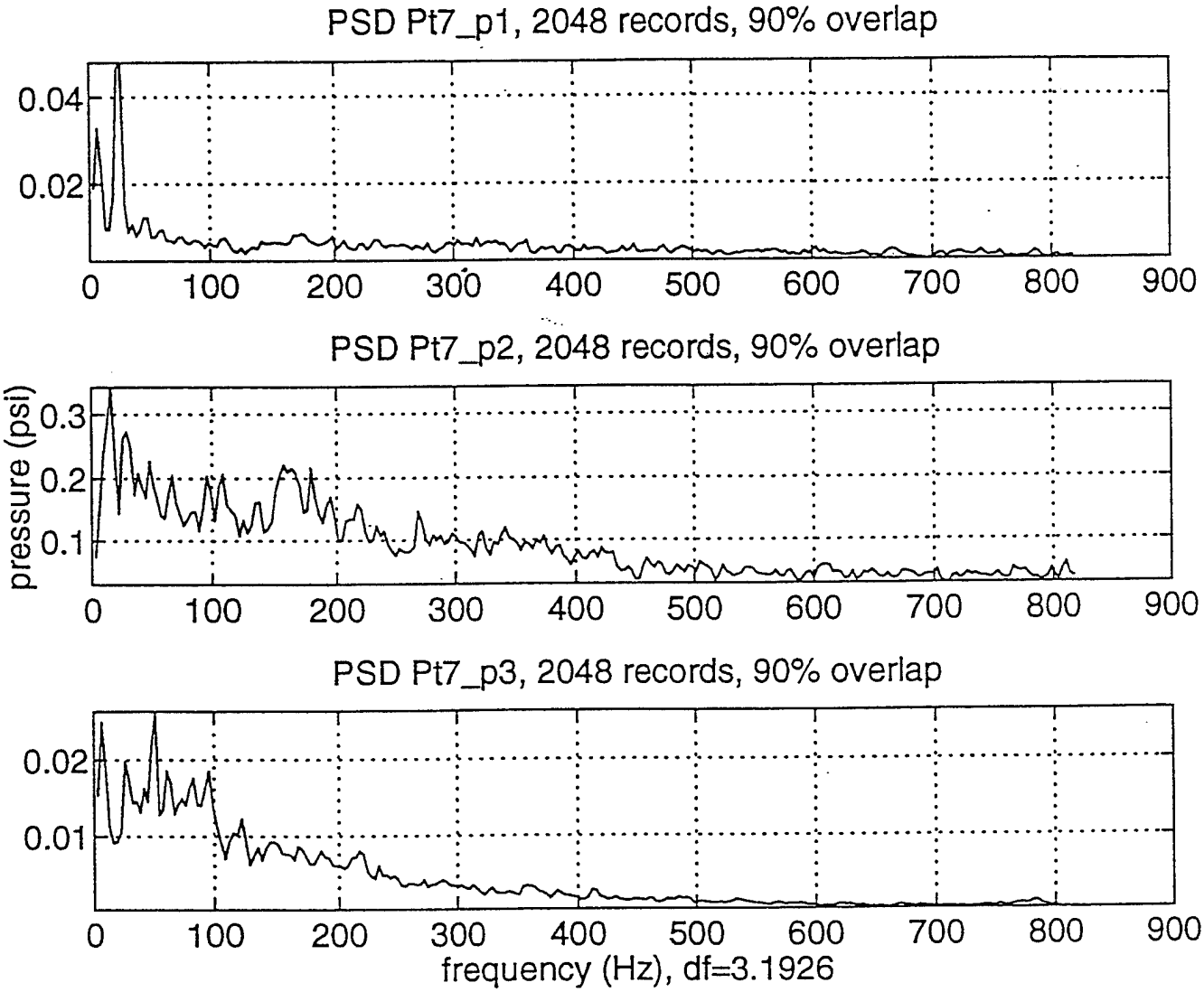
PSD Pt7_p1, 2048 records, 90% overlap
0.04
0.02
0
100
200
300
400
500
600
700
800
900
PSD Pt7_p2, 2048 records, 90% overlap
pressure (psi)
0.3
0.2
0.1
0
100
200
300
400
500
600
700
800
900
PSD Pt7_p3, 2048 records, 90% overlap
0.02
0.01
0
100
200
300
400
500
600
700
800
900
frequency (Hz), df=3.1926

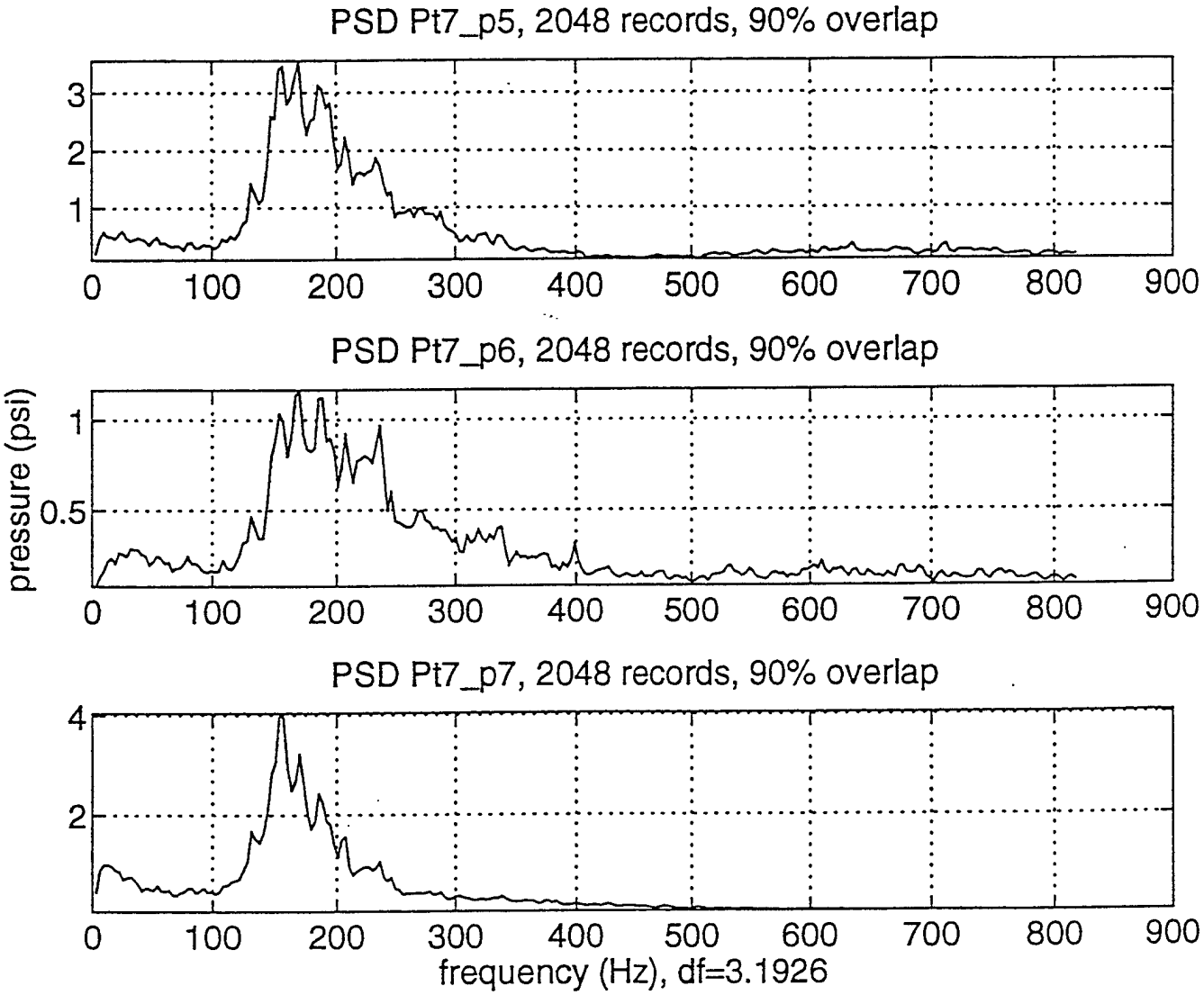
PSD Pt7_p5, 2048 records, 90% overlap
3
2
1
0
100
200
300
400
500
600
700
800
900
PSD Pt7_p6, 2048 records, 90% overlap
pressure (psi)
1
0.5
0
100
200
300
400
500
600
700
800
900
PSD Pt7_p7, 2048 records, 90% overlap
4
2
0
100
200
300
400
500
600
700
800
900
frequency (Hz), df=3.1926

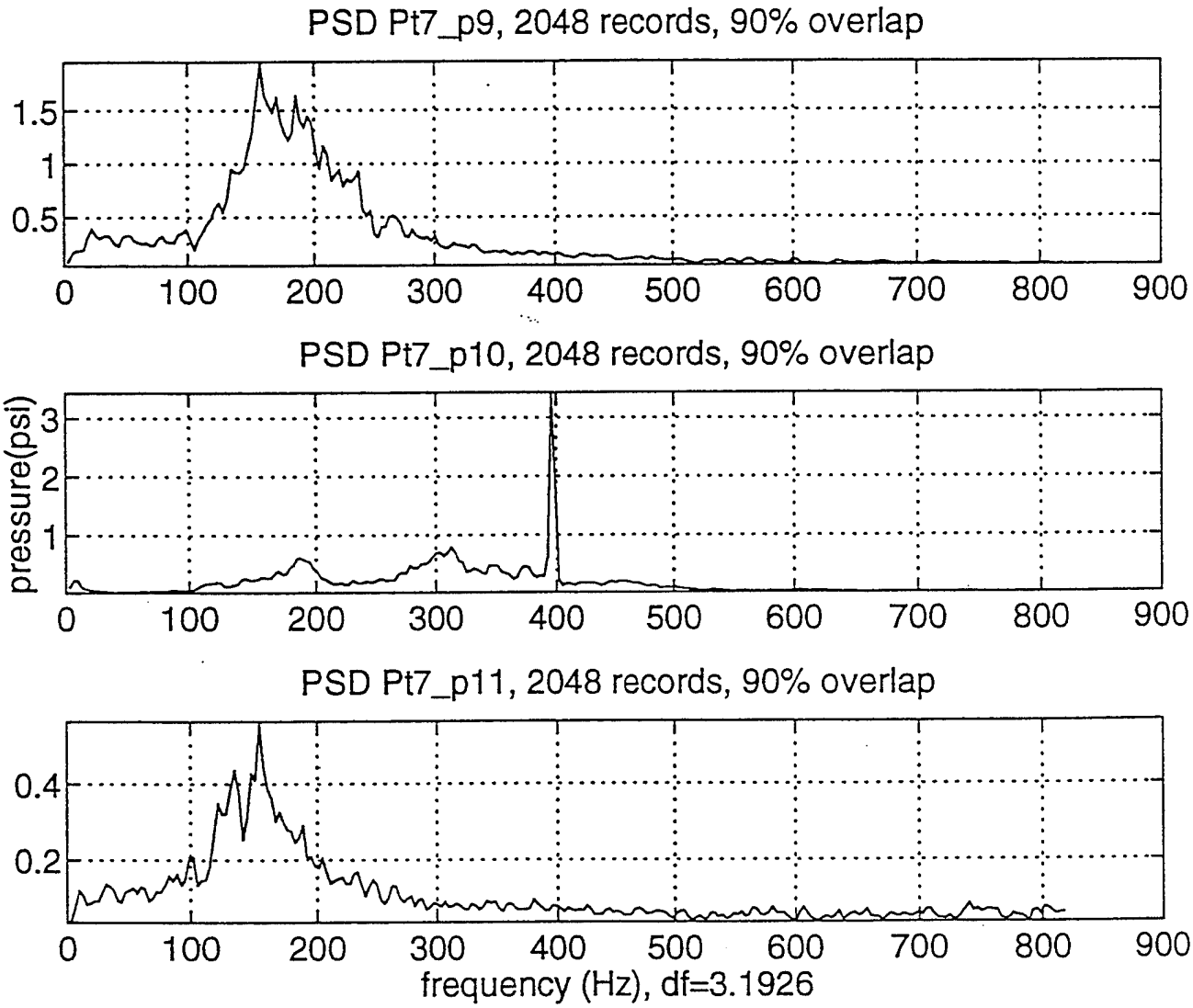
PSD Pt7_p9, 2048 records, 90% overlap
1.5
1
0.5
0
100
200
300
400
500
600
700
800
900
PSD Pt7_p10, 2048 records, 90% overlap
pressure(psi)
3
2
1
0
100
200
300
400
500
600
700
800
900
PSD Pt7_p11, 2048 records, 90% overlap
0.4
0.2
0
100
200
300
400
500
600
700
800
900
frequency (Hz), df=3.1926

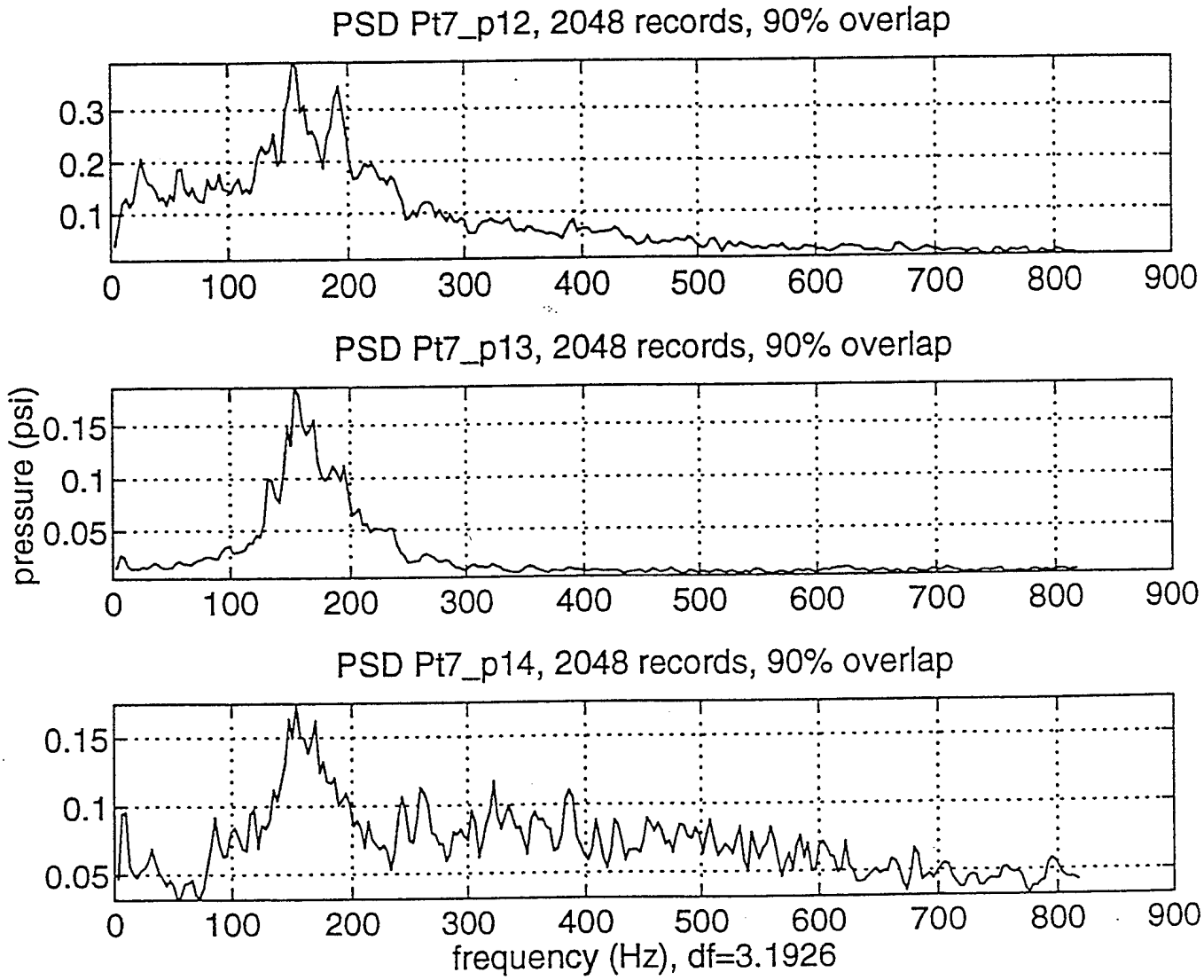
PSD Pt7_p12, 2048 records, 90% overlap
0.3
0.2
0.1
0
100
200
300
400
500
600
700
800
900
PSD Pt7_p13, 2048 records, 90% overlap
pressure (psi)
0.15
0.1
0.05
0
100
200
300
400
500
600
700
800
900
PSD Pt7_p14, 2048 records, 90% overlap
0.15
0.1
0.05
0
100
200
300
400
500
600
700
800
900
frequency (Hz), df=3.1926

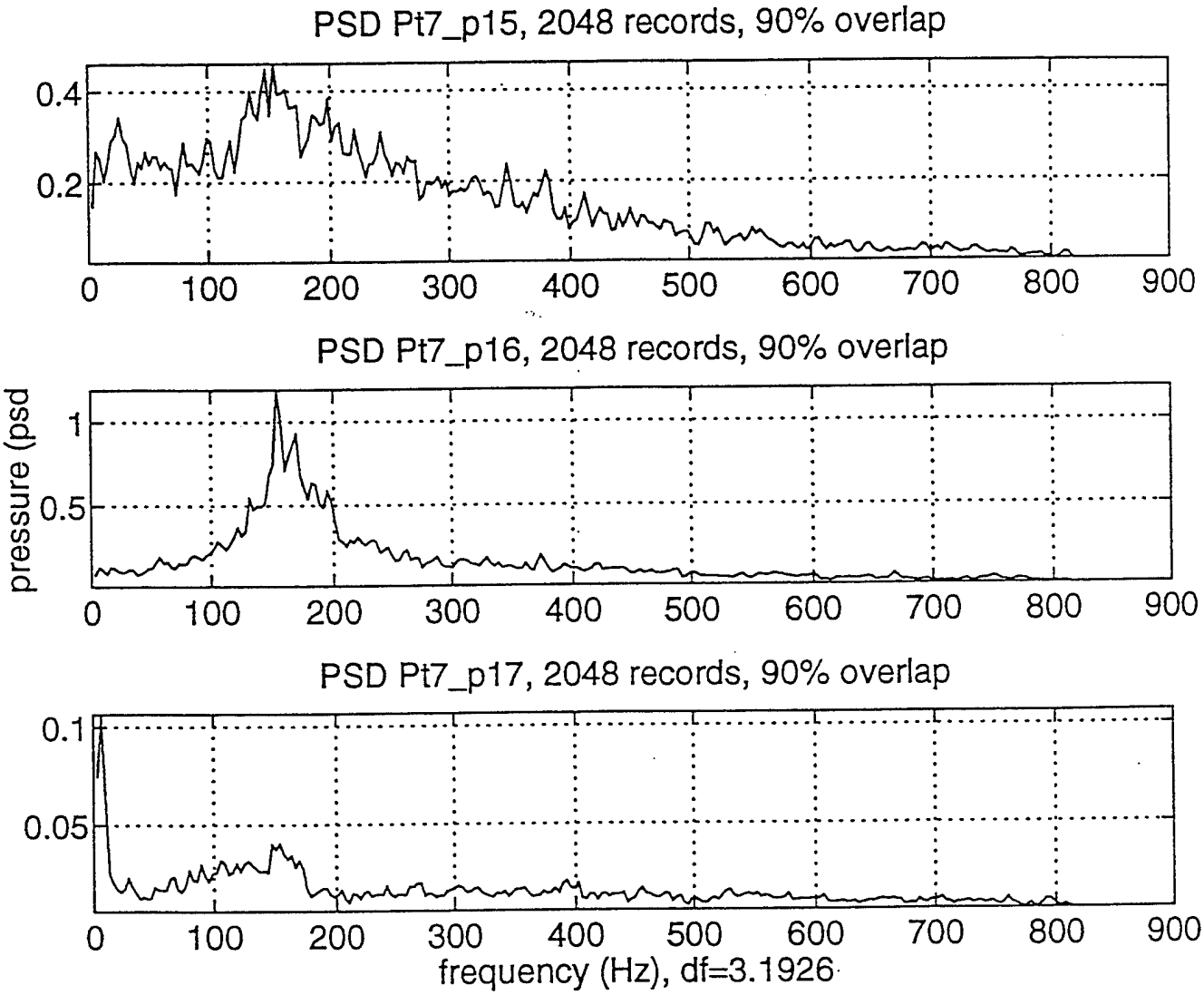
PSD Pt7_p15, 2048 records, 90% overlap
0.4
0.2
0 100 200 300 400 500 600 700 800 900
PSD Pt7_p16, 2048 records, 90% overlap
pressure (psd
1
0.5
0 100 200 300 400 500 600 700 800 900
PSD Pt7_p17, 2048 records, 90% overlap
0.1
0.05
0 100 200 300 400 500 600 700 800 900
frequency (Hz), df=3.1926